SURFACE MODIFICATION AND CHARACTERIZATION OF AGGLOMERATED METAL OXIDE PARTICLES

By
Sinan Sabuncu

Submitted to the Institute of Graduate Studies in
Science and Engineering in partial fulfillment of
the requirements for the degree of
Master of Science
in
Biotechnology

Yeditepe University
2013

SURFACE MODIFICATION AND CHARACTERIZATION OF AGGLOMERATED METAL OXIDE PARTICLES

APPROVED BY:

Prof. Mustafa Çulha
(Thesis Supervisor)

Assist. Prof. Andrew Harvey

Assist. Prof. Kaan Keçeci

DATE OF APPROVAL: .../.../....

ACKNOWLEDGEMENTS

Foremost, I would like to express my deep gratitude to my advisor, Prof. Mustafa Çulha, for his support, patience, guidance, and invaluable advice throughout my Master education.

I would like to express my great appreciation to Yeditepe University Nanobiotechnology Group Members for their support during my thesis. I'm grateful to my friends Esen Efeoğlu, Ertuğ Avcı, Mine Altunbek, Seda Keleştemur, Selda Göktaş, Manolya Hatipoğlu, Aslı Baysal, for their help and stimulating discussions during my Master education. I also would like to thank Zehra Yılmaz, Şaban Kalay, Sevda Deniz Mert, for their help and good advice. I would like to thank Assist. Prof. Kaan Keçeci for his help during my Master education.

I want to express my gratitude to Yeditepe University for giving me the opportunity to finish my thesis.

Finally, I would like to express my deepest gratitude to my parents Tarık Ahmet Sabuncu, Emel Sabuncu and Ahmet Can Sabuncu for their endless love, patience, and their confidence in me. I would also like to thank my friend Burcu Gür for her understanding and endless love.

ABSTRACT

SURFACE MODIFICATION AND CHARACTERIZATION OF AGGLOMERATED METAL OXIDE PARTICLES

Metal Oxide nanomaterials (MONMs) attracted enormous attention due to their unique physicochemical properties and are used in many applications including drugs, paints, biomedical devices and development of novel materials. The surface modification of namomaterials (NMs) is an important step to alter their behavior to further benefit from their unique properties in variety of applications. However, the main problem with them in order to work efficiently is their inefficient dispersion in aqueous environments.

In this study, we aimed to understand the surface properties of these materials as we attempt to alter the surface chemistry. Surface coating of the NMs with oligonucleotides, carbohydrates and treatment with hydrogen peroxide ($H_2O_{2)}$ help them to stabilize as mono-disperse particles in their colloidal suspensions. The characterization of modified MONMs was performed with Raman Spectroscopy, FTIR Spectroscopy and Dynamic Light Scattering (DLS).

ÖZET

TOPAKLANMIŞ METAL OKSİT PARÇACIKLARININ YÜZEY MODİFİKASYONU VE KARAKTERİZASYONU

Metal oksit nanomateryaller (MONM) özgün fizikokimyasal özelliklerinden dolayı büyük ilgi çekmektedir ve ilaç bileşenleri, boya malzemeleri, biyomedikal cihazlar ve özel materyaller gibi uygulama alanlarında kullanılmaktadır. Nanomateryallerin (NM) yüzey modifikasyonu birçok uygulamada bu materyallerin özgün özelliklerinden daha fazla yararlanabilmek için davranışlarını değiştiren önemli bir adımdır. Fakat bu malzemeler ile verimli bir şekilde çalışabilmek için karşılaşılan en büyük problem bu malzemelerin sıvı ortamlarda yetersiz dağılmalarıdır.

Bu çalışmada, bu materyallerin yüzey özelliklerinin incelenmesi ve aynı zamanda yüzey kimyalarının değiştirilmesi amaçlanmıştır. NM'lerin oligonukleotit ve karbonhidratlar ile yüzeylerinin kaplanması ve hidrojen peroksit (H_2O_2) ile muamele edilmesi bu materyallerin koloidal süspansiyonlarında tekil dağılmalarına yardımcı olduğu gözlemlenmiştir. Modifiye edilmiş MONM'lerin karakterizasyonu için Raman spektroskopisi, FT-IR spektroskopisi ve dinamik ışık saçılımı (DİS) tekniği kullanılmıştır.

TABLE OF CONTENTS

LIST OF FIGURES

LIST OF TABLES

LIST OF SYMBOLS / ABBREVIATIONS

AgNPs	Silver nanoparticles
DLS	Dynamic light scattering
DNA	Deoxyribonucleic acid
FTIR	Fourier transformed infrared spectroscopy
h	Hour
IR	Infrared
kV	Kilovolts
LSP	Localized surface plasmons
LSPR	Localized surface Plasmon resonance
mg	Milligram
MONMs	Metal oxide nanomaterials
mW	Miliwatt
MW	Molecular weight
NMs	Nanomaterials
nm	Nanometre
NPs	Nanoparticles
PBS	Phosphate Buffered Saline
PSP	Propagating surface plasmons
RNA	Ribonucleic acid
s	Second
SEM	Scanning electron microscopy
SERS	Surface-enhanced Raman scattering
SPR	Surface Plasmon resonance
SPs	Surface Plasmons
TEM	Transmission electron microscopy
UV/Vis	Ultraviolet/Visible

1. INTRODUCTION

Nano stands for dwarf in Greek and indicates a prefix in the metric system as a factor of 10^{-9} or 0.000000001. The Japanese scientist Norio Taniguchi from Tokyo University of Science was the first to use the term "nano-technology" in a 1974. In a conference he described processes such as thin film deposition and ion beam milling by using nanometer scales. He defined the word “Nano-technology” mainly as the processes of, separation, consolidation, and deformation of materials by one atom or one molecule [1].

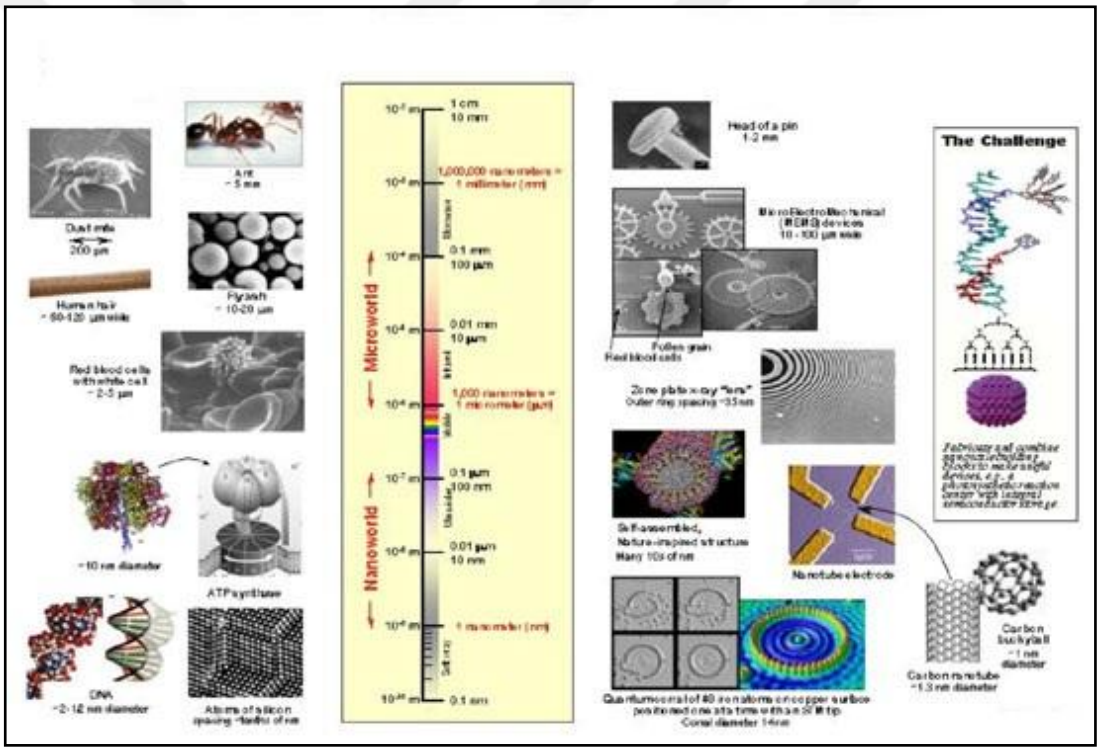

Figure 1.1. Overview of structures from nano to macroscale [2]

Nanotechnology is considered as a recent development in science but the development of its concept started over long ago. In 1980’s, nanotechnology emerged after the development of scanning tunneling microscope in 1981 and the discovery of fullerenes in 1985. These developments enabled working with nanomaterials in different fields. Nanotechnology studies materials with morphological features on the nanoscale. One of the most important properties of nanomaterials is high ratio of surface area to volume

which makes possible new quantum mechanical effects. As an example to altered quantum effect is the “quantum size effect”, where the electronic properties of solids are altered with great reductions in particle size [3].

Metal oxide nanoparticles started to be used in various applications due to their unique physicochemical properties. Metal element can form oxide compounds such as ZnO, Fe_2O_3, Fe_3O_4, TiO_2, $A_{l2}O_3$, CoAl. Main handicap of these MONMs is their possible cyto-toxic effects. Cyto-toxicity of the molecules is dependent on the size, shape and surface chemistry of the molecules. There are many synthesis procedures for these NMs and each procedure can provide different size, shape and surface properties to NMs. Since it is nearly impossible to obtain uniform size and shape in synthesized NMs, it has become popular to focus on the surface chemistry of the metal oxide NMs. There are several molecules that are being used as surface modifiers of NMs. Main goal is to reduce the toxic effect of NMs by coating them with biocompatible molecules. There are several studies about conjugation of metal oxide nanoparticles with Au and Ag NPs [4, 5], carbohydrate coating [6-8], interaction of peptides and oligonucleotides [9-11], polymer coating [12-14]. Interaction of coating materials with the NMs can be in two ways, either covalent attachment of attachment through non-covalent interactions such as hydrophobic interactions or charge interactions. Durability and the effectiveness of the coating process must be considered carefully in these kinds of studies.

For the characterization of the modified NMs, there are several instrumental analysis methods available. In order to obtain information about the size and the shape of the NMs, TEM and SEM images should be taken; DLS measurements also provide information about the dynamic radius of the NMs. Infrared (IR) and Raman Spectroscopy are two main vibrational spectroscopy types that are generally used to identify chemical composition. In order to determine the covalent modification of certain molecules on the NMs vibrational spectroscopy techniques can be used. Both techniques provide intrinsic chemical selectivity but both of them have some handicaps too. Main problem in IR spectroscopy is the absorption of infrared light by the water molecules. Due to that water-dispersed molecules cannot be studied with IR spectroscopy. In the case of Raman spectroscopy there are two main drawbacks. First one is the low signal to noise ratio for Raman signaling. Raman scattering signal is extremely weak so it needs to be enhanced by using

certain metal particles and this process is called Surface-Enhanced Raman Scattering (SERS). Also the second problem is the auto-Fluoroscence of certain molecules which can mask the real Raman signal coming from the molecule.

In this study we aimed to reduce the agglomeration and toxicity of metal oxide nanomaterials by modifying their surfaces with various biocompatible molecules such as carbohydrates, oligonucleotides, natural polymers like chitosan, hydrogen peroxide (H_2O_2). In the first part of the study, NMs were treated with hydrogen peroxide and heated in aqueous environment in order to observe the effect of hydrogen peroxide and heating on the agglomeration of NMs. In the second part of the study NMs surfaces were modified with various carbohydrates such as glucose, lactose, mannose, starch and oligonucleotides, and a natural polymer chitosan. Crosslinking by using glutaraldehyde provides a unique approach to the attachment of oligonucleotides to NMs. In order to characterize the surface modifications FT-IR and Raman spectroscopy is used.

2. THEORETICAL BACKGROUND

2.1. METAL OXIDE NMs

In the field of nanotechnology, one of the most important objectives is to make nanostructures with unique properties by using single or bulk nanomaterials. Metal oxide nanomaterials possess unique physical and chemical properties due to their high density of edge and corner surface regions [15, 16]. Size of the nanomaterials affects the basic concepts of materials in two ways. First, one is the characteristic structural properties of the materials such as lattice symmetry and cell parameters [17]. Bulk metal oxides are mostly stable systems with well-defined crystallographic structures, yet the significance of free energy and stress due to the decrease in particle size must be taken seriously. Decreasing particle size leads to the production of stress/strain in the surface atoms which can generate structural disorganizations [18]. Secondly, the sizes of the nanomaterials affect the electronic properties of the materials. The atom-like electronic states of the nanomaterials produce quantum size and confinement effects. General quantum confinement electronic effects of metal oxides are related to the energy shift of excition levels and optical band gap [19, 20]. When considered the bulk states of metal oxides, they have wide band gaps and low reactivity. However, when the size of the metal oxide nanomaterials decrease, the magnitude of the band gap and chemical reactivity also changes [21, 22].

Metal oxide nanomaterials have important role in physics, chemistry and material science [23-26]. They can be used in variety of applications like sensors, medicine, opto-electronics, catalysis [27-29]. Recent knowledge shows that the physicochemical properties of metal oxide nanomaterials are mostly related to their size alterations. Most of the applications of the metal oxide nanomaterials are related to the physicochemical properties (optical, mechanical, surface/chemistry) of the materials.

When the optical conductivity of the metal oxide nanomaterials is considered, reflectivity and absorption are the basic parameters that can be measured. Scattering of light can show important alterations when the size of the nanomaterial is in or out of the range of photon

wavelength. The absorption of the light at certain wavelengths can also give us important knowledge about the optical properties of the metal oxide nanomaterials.

Mechanical properties of metal oxide nanomaterials are mostly related with their ductility, hardness and super plasticity under low or high temperatures. Superplastic nanomaterials can undergo high value of tensile deformation without getting damaged or flawed. For example TiO_2 NMs demonstrates important compressive ductility and strain rate sensitivity at high temperatures [30].

Many metal oxide nanomaterials show acid/base and redox properties, due to those properties they are usually used in absorption and catalysis processes. These properties of the metal oxide nanomaterials generate the chemical characteristics of the nanomaterials. Surface chemistry of the NMs can be controlled with various methods and specific functional groups can be attached on the surfaces. Modified surfaces can lead to changes certain properties (optical absoprtion, size, toxicity) of nanomaterials.

2.2. AGGLOMERATION OF METAL OXIDE NMs

Dispersion of metal oxide nanomaterials (MONMs) in aqueous media has attracted a considerable amount of interest due to their potential applications including in drug systems [31], gene therapy [32], sensing [33], and paint and pigments [34]. Similar to other nanometer size materials, they tend to agglomerate and form large bundles during or after their preparation. The degree of the agglomeration is mostly governed by the synthesis method, which defines their surface properties. During synthesis processes or subsequent process steps, agglomeration of primary particles occurs as a result of weak bondings between the NMs. Then, these primary bundles form larger, strongly bonded micrometer size aggregates.

For their efficient use, the NMs should stay stable and the agglomeration should be avoided during any application process. The agglomeration can be prevented chemically and physically to a certain level [35, 36]. The use of surfactants is one of the most common ways of increasing the NM dispersion in aqueous media. Polymers such as polystyrene, poly methyl methacrylate (PMMA), and polyacrylic acid are also widely used to obtain

dispersed NMs in aqueous environments [37-39]. Although the use of these surfactants can provide higher dispersion, they contaminate the NM suspension, which may limit the applications of the NMs.

The dispersion in aqueous media can also physically be achieved with long ultrasonication processes (up to 60 h) [40]). However, the long sonication may cause erosion/dissolution and the formation of cavities on the surface of NMs [41-45]. Another external factor, temperature can be utilized for the purpose. In this respect, in several studies, the temperature dependent viscosity of nanofluids, which could be defined as solid-liquid materials established by the dispersions of NMs in the size of 1-100 nm, was examined [46]. The thermal conductivity and surface potential of the nanofluids were also studied [47-49].

2.3. SURFACE MODIFICATIONS OF METAL OXIDE NMs

Bulk and single nanomaterials show different chemical and physical properties under the same conditions. Thus, surface modifications are needed to obtain certain surface properties. Surface modifications can generate dispersion in aqueous environments when the suitable groups are attached on the surfaces of NMs [50]. Agglomeration of NMs is one of the most important problems when working with them. Surface modifications can maintain the agglomerations of the NMs [51]. Modification of surfaces of NMs can be used to obtain self-assembled NMs [52]. Certain groups on their surfaces can assist NMs to get into ordered organizations, associations.

Recently, a general concern when working with nanomaterials is their toxicity and the parameters that affect the toxicity of the NMs. Size, shape and surface chemistry determines the toxic properties of NMs. It is nearly impossible to control the uniformity of size and shape of NMs, so that surface chemistry of NMs can be considered as the most crucial parameter that reduces the toxicity. Modifications of the surfaces of NMs by using biocompatible molecules, provides opportunity to reduce possible toxic effects of certain NMs. When choosing the appropriate coating material certain properties should be considered. These properties are the proven biocompatibility, stability in various environments, chemical suitability to nanomaterial surface and the cost.

NMs can be coated with bio organic materials (carbohydrates, DNA, aminoacids and natural polymers) or synthetic materials (synthetic polymers). The main goal of surface modifications is placing desired functional groups on the surfaces of NMs. Most common groups wanted on the surfaces of NMs are thiols and disulfides [53, 54], amines and ammonium ions [55, 56], carboxylic acids [57], silanes [58, 59].

Carbohydrates are one of the most common biological molecules that are used in various applications in biology. They are made of hydrogen, carbon and oxygen which are the main components of living organisms [60]. They can be found in different structural forms in the environment and these different structures produce different carbohydrate types such as glucose, lactose and mannose etc. [61]. All of the carbohydrates can be used as coating materials for NMs but each of them will provide different properties to the NMs. Hydrophilic nature of the carbohydrates provides high dispersion in aqueous environments. Coating the hydrophobic NMs with hydrophilic carbohydrates can enhance the dispersion of NMs in aqueous environments. Carbohydrates contain various functional groups in their structure such as, ketones, aldehydes, hydroxyls, sulfates and phosphate groups. Modifications can be performed from these functional groups.

Starch is large polymer made of glucose molecules linked with glucosidic bonds [62]. Starch is made of two components, amylose and amylopectin (Figure 2.1.) [63]. Starch molecules are used as surface modifiers of NMs and they show promising results in cytotoxicity topic [64].

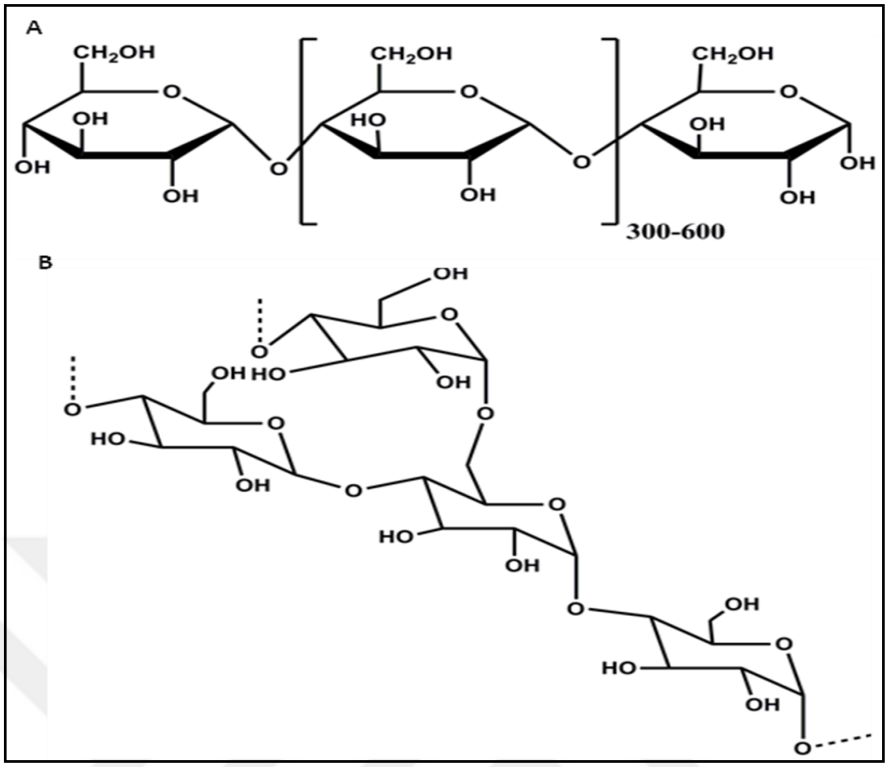

Figure 2.1. Structure of starch; amylase (A) and amylopectin (B)

Chitosan is another natural polymer made of a derivative form of chitin. In Figure 2.2. we can see the general structure of chitosan.

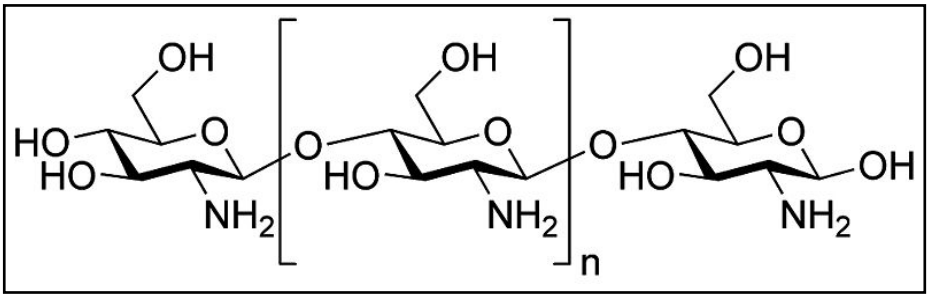

Figure 2.2. Structure of chitosan

Chitosan is a cationic polymer due to the amino groups in its structure and as a result it has higher affinity to negative molecules. Chitosan shows low toxicity and high biocompatibility in many studies [65, 66] so that it can be used in drug delivery experiments or as artificial skin, surgical sutures, and artificial blood vessels components

[67]. These properties make them favorable surface modifiers for NMs. Also chitosan has been used as the building blocks of matrixes, scaffolds, gels and fibers [68, 69]. However, its mechanical and physicochemical properties such as thermal and electrical conductivities, needed to be improved by adding organic or inorganic fillers such as calcium phosphate cements, hydroxyapatite, clay and nanoparticles [70, 71].

Oligonucleotides and peptides are important components of living systems. Oligonucleotides are usually short, single stranded DNA, made of base, five carbon sugar and phosphate backbone (Figure 2.3.). Bases of oligonucleotides can contain four different bases; adenine, timine, guanine and cytosine. Peptides are made of amino acids conjugated between each other by peptide bonds. Various peptides can be obtained by the conjugation of different amino acid sequence and length. Peptides can be modified from their N and C terminus by modifying the first and the last amino acid in the peptide sequence. As a result free functional groups can be attached on the each terminus of the polypeptides. Oligonucleotides and peptides are non-toxic and biocompatible molecules so that they can be used in various applications such as, gene delivery, tissue engineering, cosmetics, sensors, cosmetics.

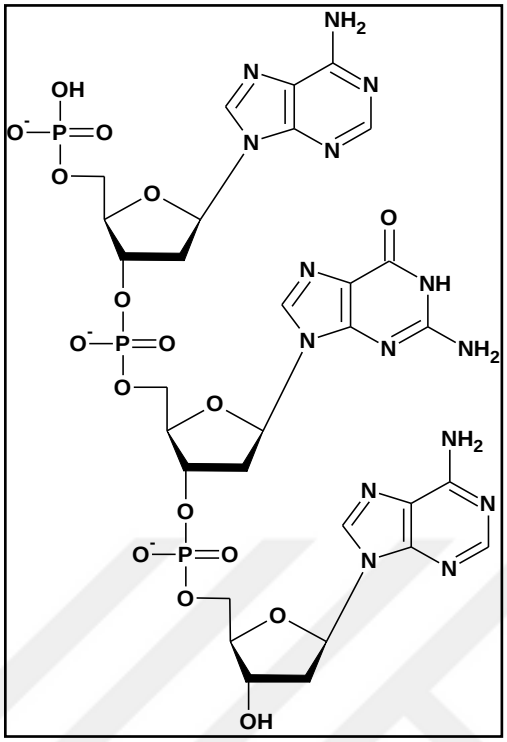

Figure 2.3. General structure of an oligonucleotide

2.4. RAMAN SPECTROSCOPY AND SURFACE ENHANCED RAMAN SCATTERING

Spectroscopy originates from the study of wavelengths of light and its interactions with matter. Light can interact with the matter in various ways such as, absorption, scattering and transmission. These interactions might cause some conformational and energetic changes in a molecule. If the incoming photons energy is high enough to excite the electrons from ground state to excited states we can say that the molecule gets excited. Absorption spectroscopy can measure the change of excitation of molecules by photons.

After the interaction of photons with matter, most of the photons scattered from molecules with the frequency of the incident radiation and this is called Rayleigh scattering. However, C.V. Raman discovered in 1928 that a very small part of the scattering has an energy shift which is different from the incident radiation and it is called Raman scattering [72, 73]. If this energy is gained it is called Stokes Raman and if it is lost antiStokes Raman. In Figure 2.4. the Jablonski diagram explains the mechanism of Raman scattering.

During Raman scattering process molecules are excited from their vibrational states to virtual states and lose energy to return to their vibrational states again. If the final vibrational states are more energetic than the initial states it is called the Stokes shift and if the final vibrational state has lower energy it is called the Anti-stokes shift.

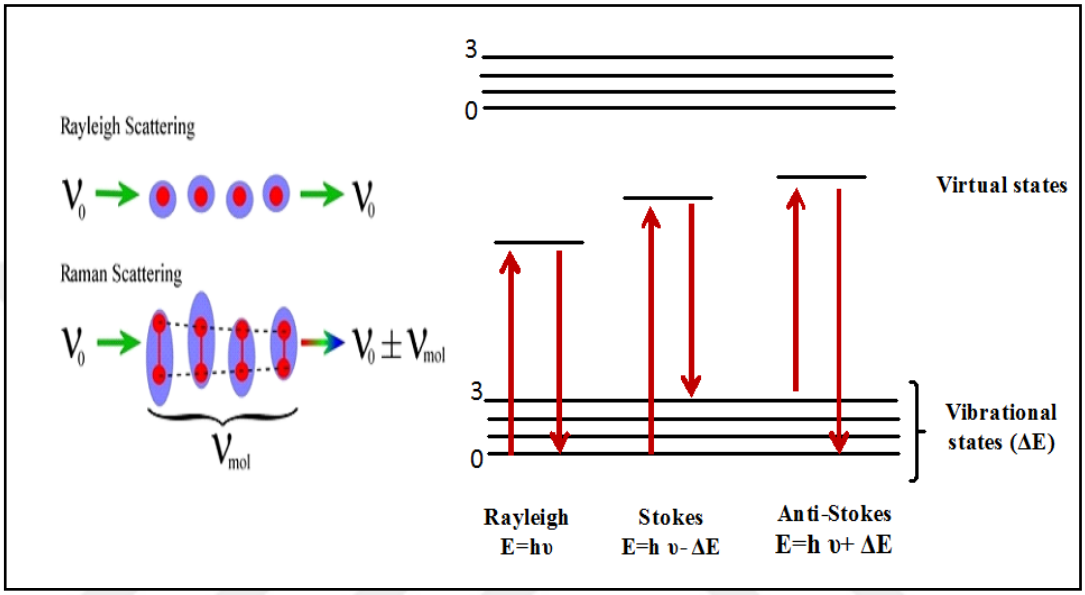

Figure 2.4. The Jablonski diagram [74]

When light interacts with the molecule and gets scattered from it some conformational changes in the molecule occur due to the formation of complexes between light and electrons. These complexes result as oscillations of electrons during Raman scattering. However, in the case of Rayleigh scattering electrons relaxes without any oscillations. These oscillations can occur in various ways like rotating and vibrating. These vibrations are derived from certain groups in molecules like carbon chains, ring formations or certain bondings. Number and the energies of the peaks give us fingerprint information about the molecule s chemical structure. As a result, we can use this important information to identify or separate specific molecules *in situ* [75, 76].

Raman spectroscopy has many advantages when compared to IR spectroscopy or other spectroscopy types. In Raman spectroscopy samples in water can be used and the sample preparation is very easy and fast. Ability to obtain fingerprint information enables the detection of multiplex molecules or single molecules in unknown solutions. The main

handicap of this technique is the weak signal of Raman scattering. Recently this problem was overcomed by the interaction of noble metal surfaces with the molecules. This technique is called surface-enhanced Raman scattering (SERS). By using this technique Raman scattering signal can be empowered 10^8 times [77-81]. The enhancement in the Raman scattering occurs on the surfaces of interacted metal nanoparticles such as silver, gold, copper, platinum and transition metals. Silver nanoparticles (Ag NPs) are the most common metal nanoparticles that are being used as SERS substrates. Their rough surfaces provide junctions and grooves where the surface plasmons are located. Surface plasmons (SPs) are known as the oscillation of electrons on metal surfaces. Surface plasmon phenomena can be divided into two groups. First one is the localized surface plasmons (LSP) and the seconds one is the propagating surface resonance (PSP) [82, 83]. Incoming light provides a force on the electrons of the metal surface and leads to the oscillation of them. When this oscillation gets into resonance with the light at certain wavelength it enhances the oscillation of the surface electrons and it is called localized surface plasmon resonance (LSPR).

3. MATERIALS

3.1. CHEMICALS

ZnO (98 nm, XRD), TiO_2 (18nm, XRD) and Fe_2O_3 (65 nm, XRD) NMs in powder form were gift from Tec Star nanofiller consultants and providers (http://www.tec-star.it). Silver Nitrate ($AgNO_3$) was purchased from Fluka. Hydrogen peroxide solution (34.5%-36.5%), trisodium citrate ($Na_3C_6H_5O_7$), glutaraldehyde (%1) was purchased from Sigma Aldrich (Germany). Carbohydrates (glucose, lactose, starch) and high molecular weight chitosan was purchased from Sigma Aldrich (Germany).

3.2. OLIGONUCLEOTIDES

Oligonucleotides were purchased from Alpha DNA (Canada) and kept in – 20 °C as 100µM. Base length and the sequences of used oligonucleotides are listed in Table 3.1. The sequences are given as from 5’ end to 3’ end.

Table 3.1. List of oligonucleotides

Label	Sequence	Base Number	Brand
PolyA-10	AAAAAAAAAA	10	Alpha DNA
PolyA-15	AAAAAAAAAAAAAAA	15	Alpha DNA
PolyA-20	AAAAAAAAAAAAAAAAAAAA	20	Alpha DNA
PolyA-25	AAAAAAAAAAAAAAAAAAAAAAAAA	25	Alpha DNA

4. METHODS

4.1. FLUORESCENCE SPECTROPHOTOMETER MEASUREMENTS

All measurements were obtained with a Cary Eclipse Fluorescence Spectrophotometer (Agilent Technologies). Excitation and emission slits were 5 nm and the PMT detector voltage was medium (600 V).

4.2. TEM MEASUREMENTS

TEM images were obtained by using JEOL-2100 HR-TEM operating at 200 kV (LaB6 filament).

4.3. ZETA SIZE (DLS and ZETA POTENTIAL ANALYSIS)

The size and zeta potential analysis were performed using Zetasizer NanoZS (Malvern, UK). It is equipped with a 633 nm 4 mW He-Ne laser. All measurements were performed in dH_2O.

4.4. PREPARATION OF SILVER NANOPARTICLES

Ag NPs were prepared by Lee and Meisel method which is based on the reduction of $AgNO_3$ salts with sodium citrate. 90 mg of $AgNO_3$ was dissolved in 500 ml of distilled water and heated until boiling. As soon as the solutions start to boil 10 ml of %1 sodium citrate was added drop by drop. After the addition of sodium citrate, solution was kept boiling until the total volume reachs the half of the initial volume. Prepared Ag NP suspension is 1x concentrated and it was concentrated to 4x concentration by a centrifugation process at 5500 rpm for 30 min and finally by removing a portion of supernatant. Produced Ag NPs were characterized with UV/Vis spectroscopy, Dynamic Light Scattering (DLS, Zetasizer) and SEM. Average size of the Ag NPs was measured as 60 nm in diameter and the maximum absorption was determined as 450 nm with UV/Vis Spectroscopy.

4.5. OLIGONUCLEOTIDE CROSSLINKING on ZnO and Fe_2O_3 NMs

A 10 ml of dH_2O was sonicated for 30 min in a falcon with open cover in order to release the free oxygen inside the sample. Then, a 30 mg of ZnO NM was added into dH_2O and sonicated for 30 min. Prepared ZnO suspension was mixed with 10 µl of oligonucleotide (10, 15, 20, 25 Adenine base pair) and 500 µl of glutaraldehyde (%1). Final suspension was put in a volumetric flask and put on a hot plate (Heidolph MR 3004, Germany), which was previously heated to 40 °C, while stirring. Suspension was left for 2 hours under N2 exposure, on the heater.

Obtained oligonucleotide attached NMs were washed 3 times with dH_2O and dialyzed overnight in a dialysis tubing cellulose membrane (flat width 25 mm) which retains particles over 12.400 Mw with %90 efficiency.

4.5.1. Crosslinking of Starch, Chitosan and Lactose on TiO_2 and Fe_2O_3 NMs

A 10 ml of dH_2O was sonicated for 30 min in a falcon with open cover in order to release the dissolved oxygen inside the sample. Then, a 30 mg of desired NM was added into dH_2O and sonicated for 30 min. The prepared NM suspension was mixed with 10 mg of starch, chitosan or lactose and 500 µl of glutaraldehyde (%1). Final suspension was put in a volumetric flask and put on a hot plate (Heidolph MR 3004, Germany), which was previously heated to 40 °C, while stirring. Suspension was left for 2 hours under N_2 exposure, on the heater.

The surface coated NMs were washed 3 times with dH_2O and dialyzed overnight in a dialysis tubing cellulose membrane (flat width 25 mm) which retains particles over 12.400 Mw with % 90 efficiency.

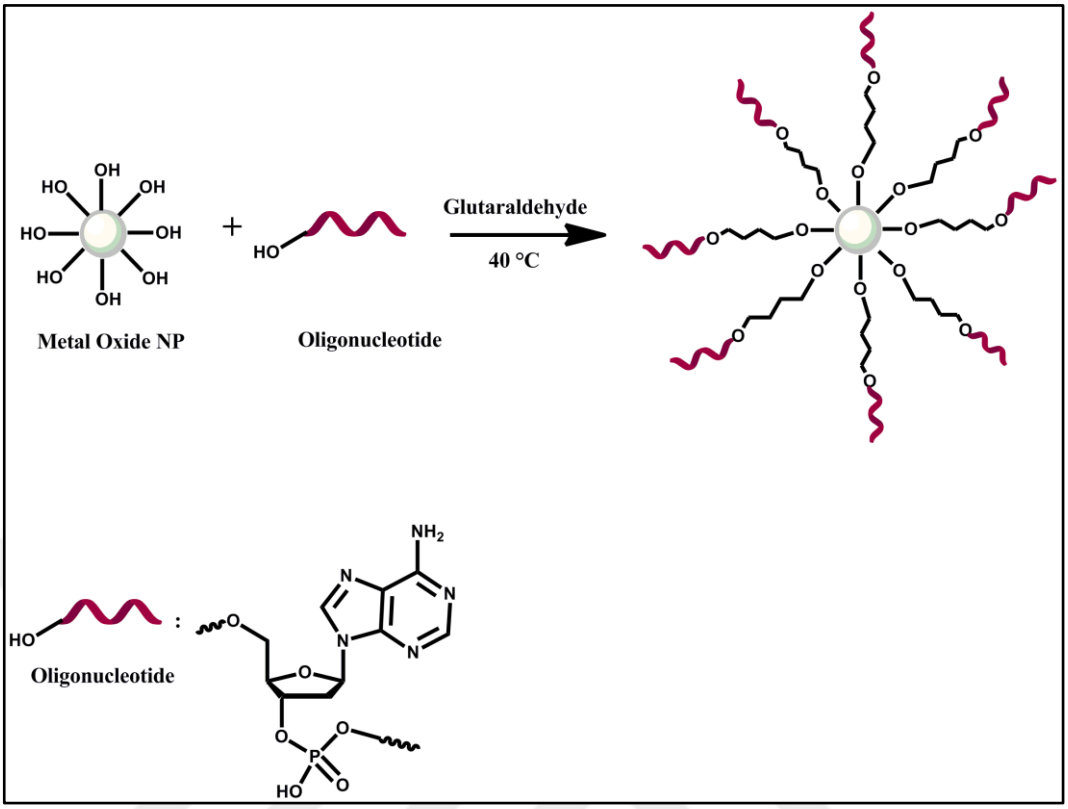

Figure 4.1. Crosslink process of oligonucleotide on the metal oxide surfaces

4.6. HYDROXYLATION OF ZnO and TiO_2 NMs by H_2O_2

0.2 grams of ZnO and TiO_2 NMs were weighted and dispersed in 25 ml H_2O_2 solution. The resulting NM suspension was left to dry on a hot plate (Heidolph MR 3004, Germany), which was previously set to 300 hot plate scale and kept boiling until all of the solvent evaporated. For the washing step, the obtained NM powder was dispersed in 10 ml of distilled water (dH_2O) and left for drying on a hot plate, which was previously set to the 300 scale. Finally, the hydrogen peroxide treated NMs were obtained in powder form. The NMs were re-dispersed in dH_2O and stored at room temperature.

4.7. HEATING HYDROXYLATED ZnO and TiO_2 NMs

Hydroxylated ZnO or TiO_2 NMs were added into dH_2O (1 mg/mL). The prepared suspensions of NMs were sonicated for 30 min. Then, sonicated suspensions were left to rest in order to obtain a saturated aqueous suspension. After the resting phase, supernatant of the suspension was transferred to a centrifuge tube and stored at room temperature. All experiments were performed from the same batch.

The agglomeration state of the bare and hydroxylated NMs was evaluated with temperature gradient from 30°C to 90 °C with 5 °C intervals. Between each interval of 5 min of equilibration time was used regardless of the time spent by the instrument to set the temperature. The suspension was placed into a folded capillary cell for zeta potential measurements and zeta potentials of NMs were measured at 30 °C. All experiments were performed at least 3 times.

4.8. FOURIER TRANSFORM INFRARED SPECTROSCOPY (FT-IR) ANALYSIS

FTIR analysis was performed with Thermo Scientific Nicolet iS50 FT-IR (Massachusetts, USA) in attenuated total reflectance (FTR) mode with a diamond plate and ZnSe lens. Samples were dried at 90 °C on a hot plate before analysis.

4.9. RAMAN SPECTROSCOPIC MEASUREMENTS

A Raman Microscopy System (InVia Reflex, Renishaw, UK) was used to perform all SERS experiments. The system was used with a diode laser at 830 nm and at 514 nm with a 50X objective. The system was automatically calibrated by using a silicon wafer peak at 520 cm^{-1}. Laser power was 3mW at the sample position. Exposure time was 20 seconds for the elimination of coating materials on NMs experiments and 10 seconds for the rest of the measurements. Ten spectra were acquired from each sample and each experiment was repeated for at least 3 times.

4.9.1. Investigation of The Presence of Coating on NMs by Using Raman Spectroscopy and SERS

In order to eliminate the coated biological materials on the NMs diode laser at 514 nm was used. Biomolecules on the surfaces of NMs were exposed to the laser power and melted. The change in the Raman and SERS spectra of NMs was investigated while the biomolecules on the surfaces start to melt down.

The samples were mixed with 4X Ag NMs for the SERS measurements and the bare samples were used for the Raman measurements. Exposure time was 20 seconds and laser power was 3mW for each measurement. 50 measurements were taken from the same spot of the sample and results are recorded after each measurement in order to understand any possible changes in the bands after exposure to laser power. The same procedure was performed for the Raman measurements without using Ag NMs.

5. RESULTS AND DISCUSSION

5.1. CHARACTERIZATION of NMs

ZnO, TiO_2 and Fe_2O_3 NMs, which were used in this study, were characterized with TEM, Raman Spectroscopy, FT-IR Spectroscopy, Fluorescence Spectroscopy and DLS measurements.

5.1.1. ZnO NMs

As seen in Figure 5.1. A, the size of ZnO NMs were determined approximately 90 nm.

Bare ZnO NMs have also characterized by using Raman spectroscopy. Raman spectroscopy provides important information about molecules and molecular structures due to high spatial resolution and narrow spectral bandwidth. As it is seen in Figure 5.1.B, bulk Raman spectra of the NMs shows the characteristic bands of ZnO NMs such as 1090 cm^{-1}, 390 cm^{-1} and 1380 cm^{-1} which are related to the crystal structure of ZnO NMs

After the characterization of ZnO NMs with Raman Spectroscopy, further characterization was made by using FT-IR spectroscopy to determine possible functional groups on the surfaces of NMs. FT-IR can provide valuable information about the surface properties of NMs. Therefore the comparison of bare and modified ZnO NMs can be used to identify completion of modification process. Figure 5.1.C, shows the bare ZnO NMs FT-IR spectrum. The bands that belong to any functional group were not observed on bare ZnO NMs.

As a final characterization step, excitation and emission spectra were acquired and fluorescence properties of ZnO NMs were controlled by using Fluorescence spectroscopy. Figure 5.4.represents the emission spectrum of ZnO NMs. The emission wavelength of ZnO NMs was determined as 410 nm while excitation wavelength was 385 nm.

These characterizations give important information on the surface properties of ZnO NMs and their size. Characteristic data of bare NMs can be further used to analyze surface modified NMs by comparing them between each other.

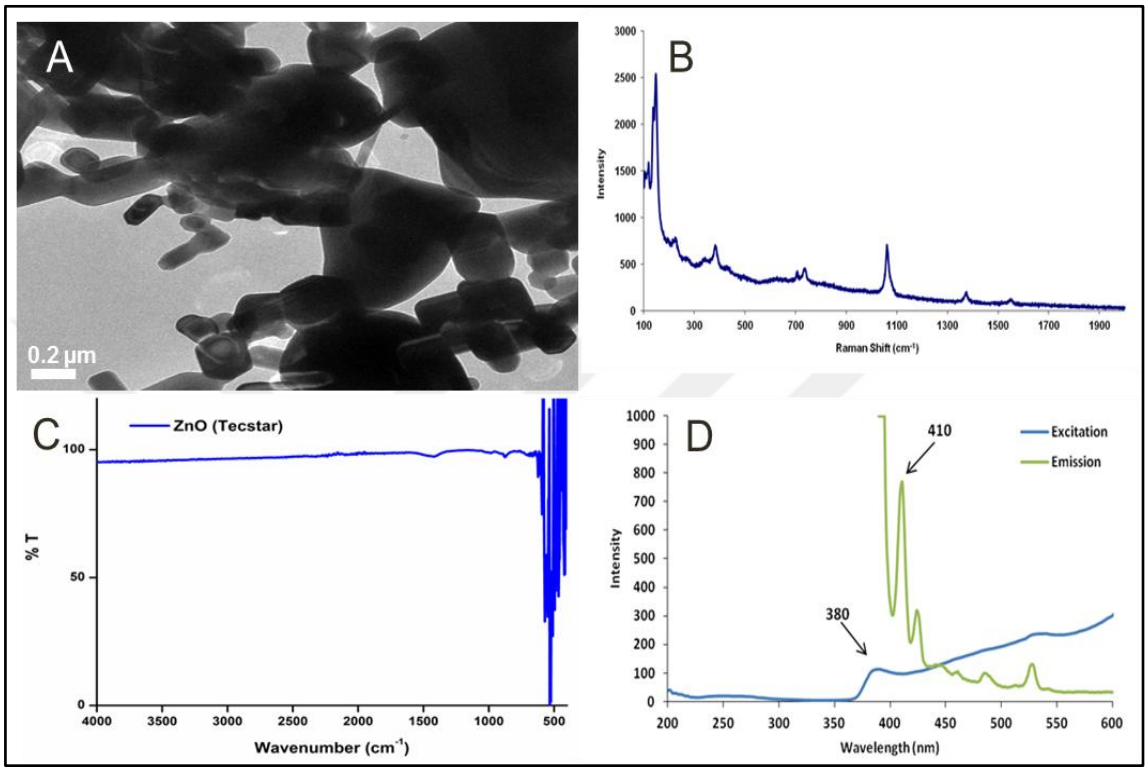

Figure 5.1. TEM image (A), Raman spectrum (B), FT-IR spectrum (C), Excitation and emission spectrum (D) of ZnO NMs

5.1.2. Fe_2O_3 NMs

As seen in Figure 5.2. A, the size Fe_2O_3 NMs were determined approximately 30 nm.

Fe_2O_3 NMs were characterized by Raman spectroscopy in order to obtain important information about the NMs surfaces and their electronic structure. Figure 5.2.B shows bulk-Raman spectra of bare Fe_2O_3 NMs. The characteristic bands of Fe_2O_3 NMs are 280 cm^{-1}, 300 cm^{-1}, 400 cm^{-1}, 490 cm^{-1}, 600 cm^{-1}, and 1310 cm^{-1}**.** Comparison of the intensities of characteristic bands of bare NMs and modified NMs can provide information about the effect of the surface modifications on the oscillation of surface electrons of NMs.

In order to obtain information about the surface properties of Fe_2O_3 NMs FT-IR spectroscopy was used. From the Figure 5.2.C we can observe the broad band at around 3600 cm^{-1} which is generally originated from the –OH groups. The presence of the –OH groups on the surfaces of NMs may allow further modification of the material. Other bands on the FT-IR spectra of Fe_2O_3 NMs can be due to the impurities on the surface of NMs, originating from synthesis procedure.

Finally Fe_2O_3 NMs were characterized with fluorescence spectroscopy. Fe_2O_3 NMs were scanned from in order to determine the excitation wavelength of NMs. The prescan measurement which scans from 200 nm to 800 nm wavelength shows that the NMs get excited only at 620 nm wavelength. The emission value of Fe_2O_3 NMs, after the excitation by 620 nm wavelength of light, was measured. From Figure 5.2.D we can see that the Fe_2O_3 NMs do not have any emission at 620 nm excitation value. So it can be stated that the Fe_2O_3 NMs do not have fluorescence properties.

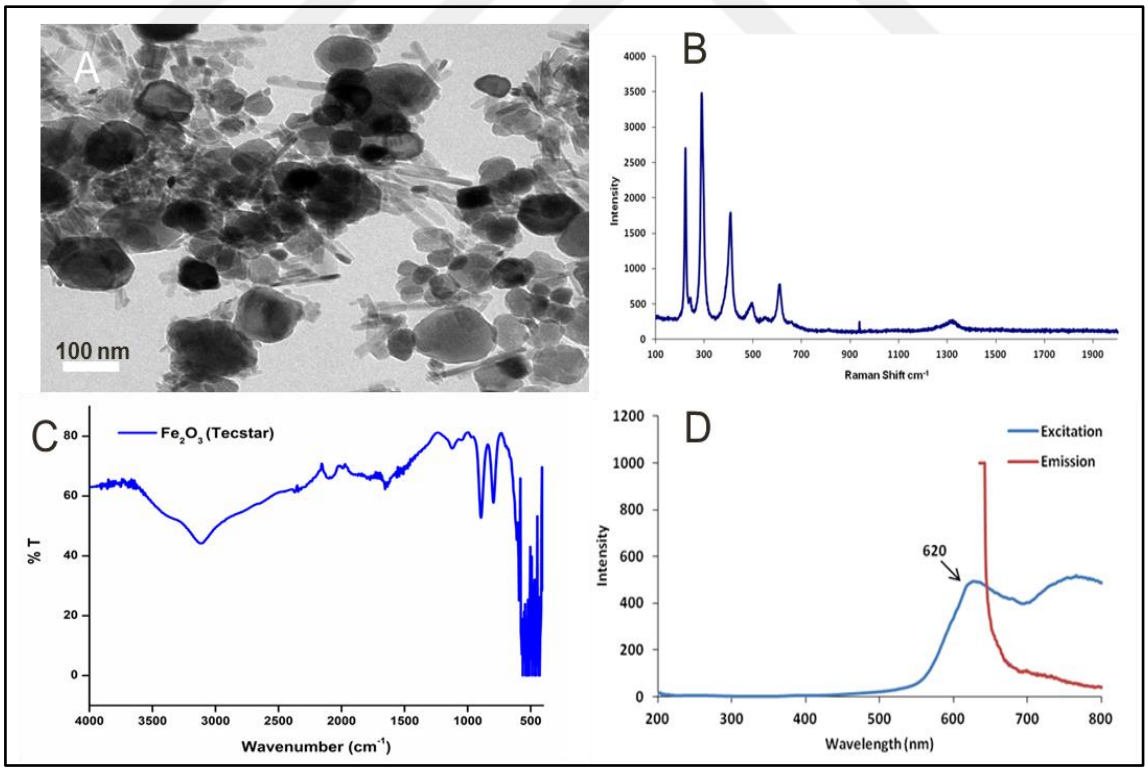

Figure 5.2. TEM image (A), Raman spectrum (B), FT-IR spectrum (C), Excitation and emission spectrum (D) of Fe_2O_3 NMs

5.1.3. TiO_2 NMs

As seen in Figure 5.3. A, the size TiO_2 NMs were determined approximately 40 nm. Raman spectroscopy provides characteristic information about TiO_2 NMs. This knowledge can be further used to identification and characterization of intrinsic properties of coated TiO_2 NMs. Figure 5.2.B shows bulk-Raman spectra of bare TiO_2 NMs. The characteristic bands of TiO_2 NMs are observed at 120 cm^{-1}, 420 cm^{-1}, 510 cm^{-1} and 690 cm^{-1} as seen in the Figure.

For the characterization of the surface properties of the TiO_2 NMs FT-IR spectroscopy was used. It can be seen from the Figure 5.3.C that TiO_2 NMs do not contain impurities on their surfaces. The broad band at 3600 cm-1 shows the presence of – OH groups on the surfaces of NMs.

In order to investigate the fluorescence properties of TiO_2 NMs, fluorescence spectroscopy was used. Figure 5.3.D represents the excitation and emission spectrum of TiO_2 NMs. Excitation wavelength of TiO_2 NMs is 385 nm and emission wavelength is at 410 nm.

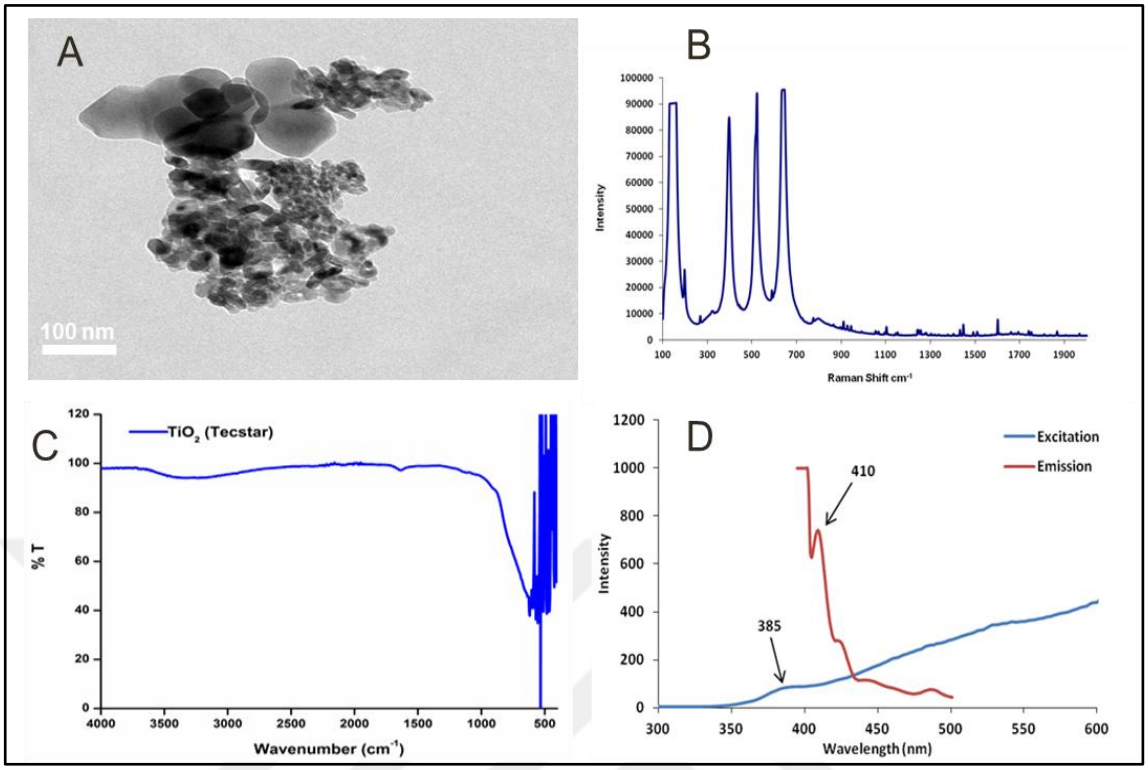

Figure 5.3. TEM image (A), Raman spectrum (B), FT-IR spectrum (C), Excitation and emission spectrum (D) of TiO_2 NMs

By using the results of these characterization techniques, it was observed that these NMs are individually extremely small (30- 100 nm) in size and due to that they tend to agglomerate and form large aggregates. Also, from the FT-IR spectroscopy results it was observed that the surfaces of bare TiO_2 and Fe_2O_3 NMs contain –OH groups. However, bare ZnO NMs do not contain any –OH groups on their surfaces. As a result bare Fe_2O_3 and TiO_2 NMs have higher dispersion in dH_2O than bare ZnO NMs.

5.2. H_2O_2 TREATMENT OF ZnO and TiO_2 NMs

5.2.1. Variations in the zeta potentials of NMs after hydroxylation

Zeta potential (ζ) of NMs provides information about the surface charge of the particle in a solvent. Surface charge of a particle can vary with respect to the change in their environment or any change in the surface chemistry. The hydroxylation process introduces hydroxyl groups (-OH) on the surfaces of NMs [84]. Figures 5.4 and Figure 5.5 shows the

FT-IR spectra of ZnO and TiO_2 NMs before and after the hydroxylation process, respectively. Since all samples were dried on a hot plate to remove any remaining water in the samples, it is clear from Figure 5.4 that the intensity of the characteristic IR absorption frequency of –OH is between 3200-3600 cm^{-1} increases after the hydrogen peroxide treatment, which indicates the increase of the –OH density on the ZnO NP surfaces after H_2O_2 treatment It was not expected to introduce further -OH on the TiO_2 NP surfaces after the hydroxylation process, since the surfaces of bare NPs already contain –OH groups. Thus from Figure 5.5 it can be observed that there is not a significant change in the broad –OH band between 3200-3600 cm^{-1}. Although, there is almost no difference on the FTIR spectra of TiO_2 NPs before and after the hydrogen peroxide treatment, the change in zeta potential suggests an alteration on the surface property of the TiO_2 NPs. This might be the result of removal of organic impurities remaining from the synthesis on the NPs and indicates the presence of –OH groups on the surfaces of bare TiO_2 NPs. Table 1 shows the changes in the zeta potential of ZnO and TiO_2 NPs before and after the hydroxylation process. The resulting hydroxylated NPs become rich in –OH groups on the surface, which results in the shift of the zeta to more negative relative to untreated NPs.

Table 5.1 shows the changes in the zeta potential of ZnO and TiO_2 NMs before and after the hydroxylation process. The resulting hydroxylated NMs become rich in –OH groups on the surface, which results in the shift of the zeta to more negative relative to untreated NMs.

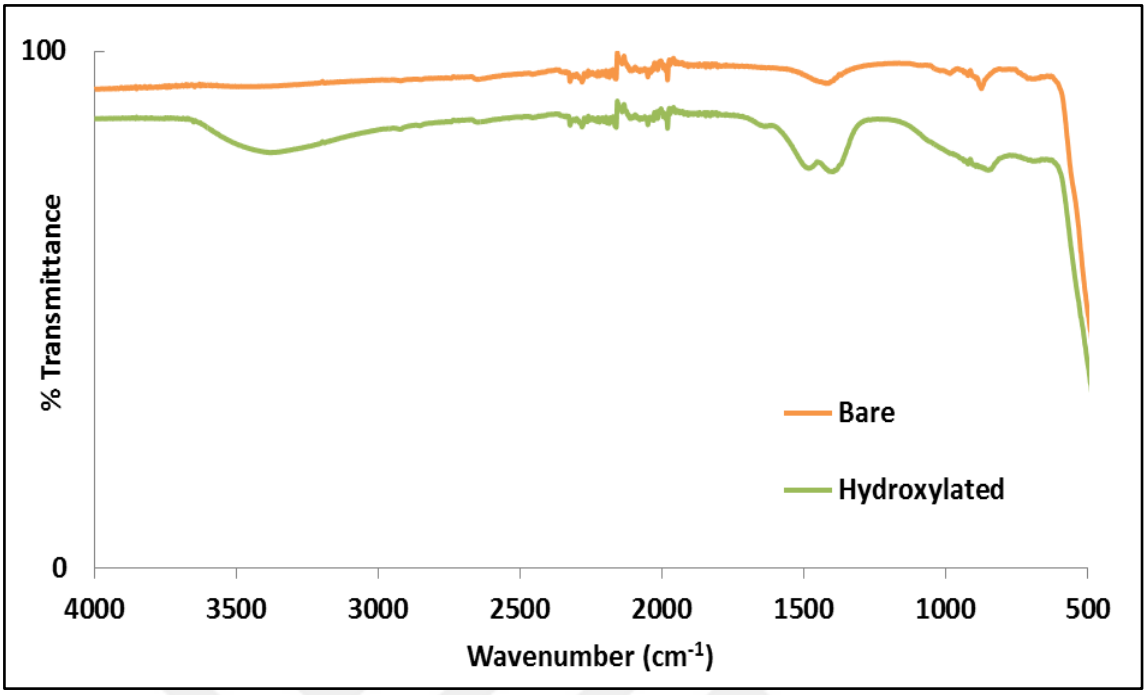

Figure 5.4 Comparison of FT-IR spectra of bare and hydroxylated ZnO NMs

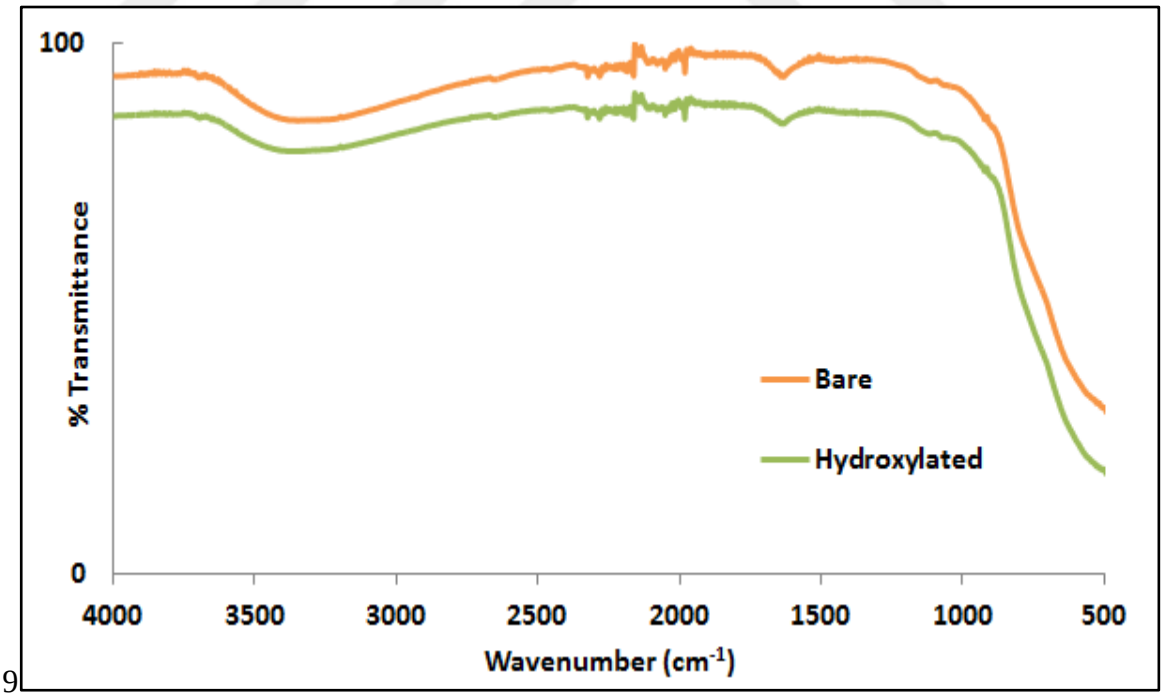

9

Figure 5.5. Comparison of FT-IR spectra of bare and hydroxylated TiO_2 NMs

Table 5.1. Zeta potentials of bare ZnO, TiO_2 NMs and hydroxylated ZnO, TiO_2 NMs

	Zeta Potential / mV (30°C)
Bare ZnO NMs	63,3 ∓ 0,70
Hydroxylated ZnO NMs	23,3 ∓ 1,13
Bare TiO_2 NMs	81,5 ∓ 0,212
Hydroxylated TiO_2 NMs	32,5 ∓ 0,012

5.2.2.

Temperature dependent size distribution of hydroxylated NMs

The TiO_2 and ZnO NMs used in the study have poor dispersion in dH_2O, and when suspensions of these NMs are prepared, large clusters and aggregates are observed. After 30 min. of sonication, their dispersion is slightly improved in dH_2O and after a short time (in 10 min) the NMs are precipitated.

The effects of heating and treatment with hydrogen peroxide on the size distribution of the ZnO and TiO_2 NMs were investigated by measuring hydrodynamic radii of the NMs in their suspension in water. Figure 5.6 shows the temperature dependent hydrodynamic radii change of the bare and hydroxylated TiO_2 NMs. As mentioned above, the hydroxylation process removes possible impurities from the NM surfaces and increases the density of –OH groups on the surface. Therefore, the NMs are better dispersed in dH_2O. Figure 5.6 a shows the change in the hydrodynamic radii of the hydroxylated TiO_2 NMs with increasing temperature. At 30-40 °C, the aggregates of TiO_2 NMs also exist in very large size (in the micrometer range) and a wide range of size distribution, and therefore, the standard deviation of the measurements are also high. This is due to the presence of large clusters and hydroxylation provides slightly better dispersion in dH_2O. As the temperature is increased, the decrease in the hydrodynamic radii of the treated TiO_2 NMs is clearly observed. At 90 °C, we obtain the size of ~120 nm, which we can consider them as primary NMs. It can be concluded that the most significant decrease in the hydrodynamic radii of the TiO_2 NMs occur after 80 °C. In order to see that these changes in the

hydrodynamic radii of the TiO_2 NMs are related to the hydroxylation or temperature effect, the experiment is repeated with the bare TiO_2 NMs. Figure 5.6 b shows the temperature dependent hydrodynamic radii change of the bare TiO_2 NMs. In this case, the hydrodynamic radii of the bare TiO_2 NMs decrease by the increasing temperature but the smallest size obtained is around ~290 nm and the standard deviations of the measurements are higher, which indicates a large variation in the aggregate sizes. The bare TiO_2 NMs suspension contains large micrometer size clusters in the range of 30 to 40 °C, and between 50 and 90 °C, the size decreases to the range of 300-500 nm.

In Figure 5.6 c, the comparison of the change in the hydrodynamic radii of hydroxylated and bare TiO_2 NMs with increasing temperature is seen. The hydrodynamic radii of the hydroxylated TiO_2 NMs are smaller when compared to the bare TiO_2 NMs at each temperature interval. The large standard deviations in the case of bare TiO_2 NMs indicate the poly-dispersion of the particles in the suspension. The hydrodynamic radii of the hydroxylated TiO_2NMs decreased % 91.7 (from 1484 nm to 122 nm) and for the bare TiO_2 %80.1 (from 1484 nm to 295 nm) when the temperature was increased from 30 °C to 90 °C. After 60 °C this difference observed more clearly, from 60 to 90 °C, the decrease in hydrodynamic radii of the hydroxylated and the bare TiO_2 NMs is %69.1 and %35.5, respectively.

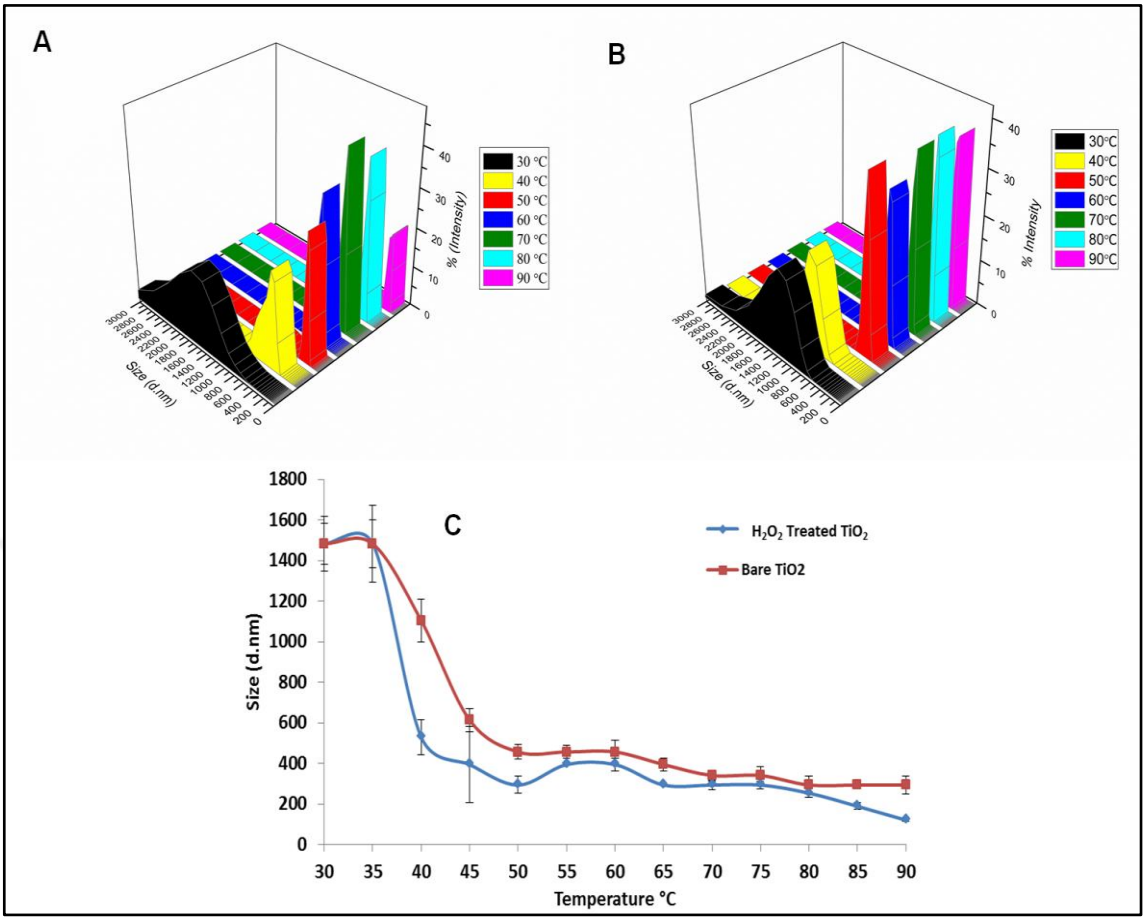

Figure 5.6. Temperature dependent size change of H_2O_2 treated TiO_2 NMs (A), bare TiO_2 NMs (B) and Temperature – Size change graph of bare and H_2O_2 treated TiO_2 NMs (C)

The bare ZnO NMs have lower dispersion in dH_2O when compared to bare TiO_2 NMs. Even after 30 min. of sonication they are poorly dispersed and precipitated faster than TiO_2 NMs. Thus, it becomes difficult to work with bare ZnO NMs in dH_2O.

The ZnO NMs were hydroxylated with the same procedure as TiO_2 NMs and the effect of hydroxylation on the hydrodynamic radii of the NMs was much clearer in the case of ZnO NMs. By comparing Figure 5.7 a and b, it can be seen that the hydrodynamic radii of the hydroxylated ZnO NMs is significantly smaller than the bare ZnO NMs at each temperature point. The hydrodynamic radii of the bare ZnO NMs is around 900-1200 nm until the temperature increases to 40 °C but after that it increases to ~2000 nm at 50 °C and gets smaller until it reaches 90 °C. This can be explained by the lack of dispersion of bare ZnO NMs in dH_2O. The bare ZnO NMs tend to form larger clusters than the bare TiO_2

NMs are in dH_2O and precipitate much faster, thus the average size deviation is higher with the bare ZnO NMs.

The hydroxylated ZnO NMs show a more gradual decrease in hydrodynamic radii when the temperature increases. From Figure 5.7 a, it can be seen that the hydroxylated ZnO NMs are around 1000 nm at 30°C - 40 °C and gets smaller by increasing temperature and eventually it reaches to ~280 nm at 90 °C. When the size of one ZnO NMs is ~98 nm is considered, the obtained ~280 nm of hydrodynamic radii shows that the NMs form aggregates by combination of a few NMs. It is clearer in Figure 5.7 c that when the hydroxylation and heating is combined the hydrodynamic radii of ZnO NMs gets smaller. At 90 °C most of the aggregates in the ZnO suspension breaks down and primary particles are obtained. Figure 5.7 c shows the change in the size of bare and hydroxylated ZnO NMs at each temperature intervals. Due to the very low dispersion of bare ZnO NMs in dH_2O, the size variation is very high. The uncontrollable precipitation of bare ZnO NMs leads to the irregular size change when the temperature increases. However, in the case of the hydroxylated ZnO NMs, there is a steady decrease in the size of the NMs when the temperature increases. When the temperature was increased from 30 °C to 90 °C, a % 73. 2 decrease in the hydrodynamic radii of the hydroxylated ZnO NMs and a % 51.9 decrease in the size of the bare ZnO was observed. After 60 °C, the profile change in the size of both bare and hydroxylated ZnO NMs are observed to be similar. From 60 °C to 90 °C, the decrease in the size of the hydroxylated ZnO NMs (from 955 nm to 255 nm) is %35,6 and for the bare ZnO NMs, it (from 1106 nm to 531 nm) is %44,3. The percent decrease in the case of bare ZnO NMs is higher but the final size of the bare ZnO (531 nm) is more than %50 larger than the size of hydrogen peroxide treated ZnO NMs (255 nm).

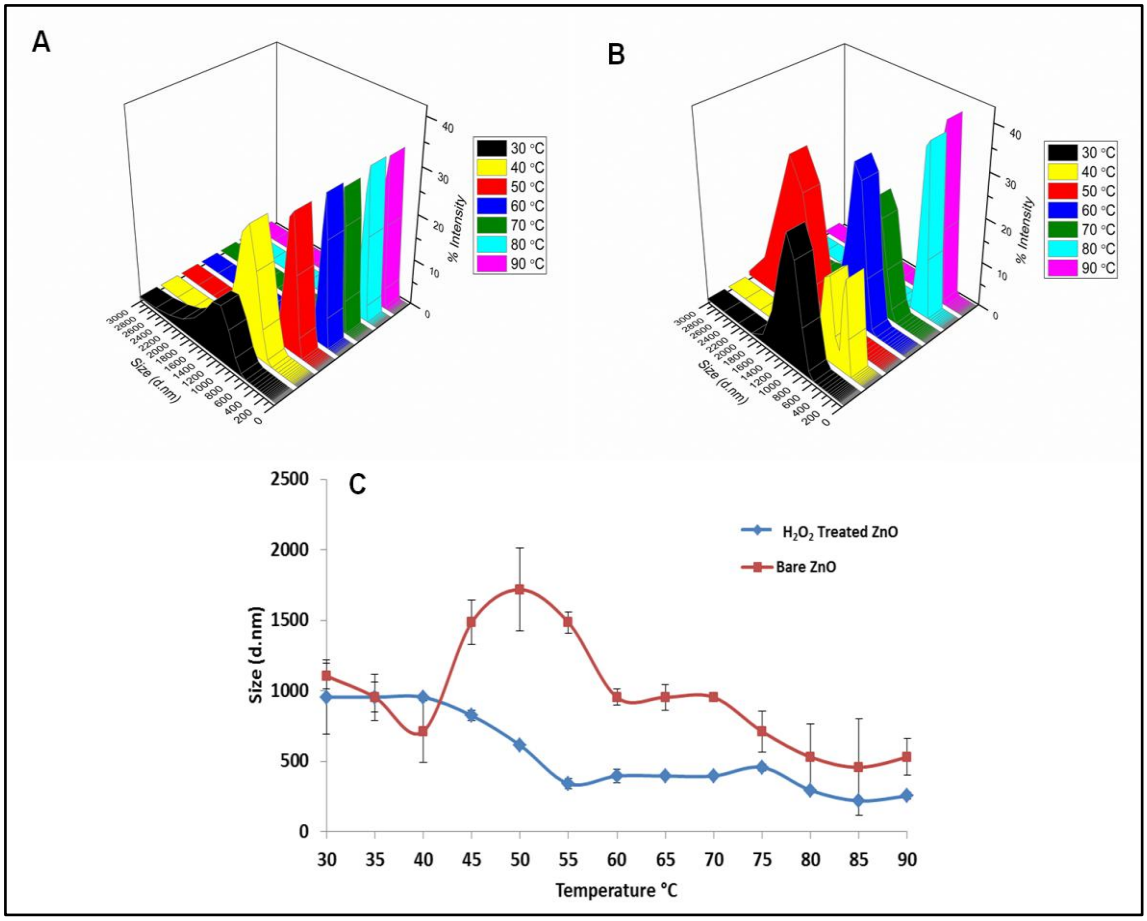

Figure 5.7. Temperature dependent size change of H_2O_2 treated ZnO NMs (A), bare ZnO NMs (B) and Temperature – Size change graph of bare and H_2O_2 treated ZnO NMs (C)

The aggregation profiles of the suspension from the area of dried droplet can provide valuable information about the cluster size in their suspension. Although much of the particles are accumulated at the liquid-solid-air interface of a droplet due to "coffee-ring phenomenon" [85], particles escapes from the outward solvent flow inside of a drying droplet precipitates in middle region of the dried droplet. Therefore, a 2 µL of the suspension was placed on a glass slide and let it dried. The SEM images from the middle region of the droplet acquired. SEM images of bare ZnO and TiO_2 NMs at 30 °C and 90 °C were compared with the hydroxylated ZnO and TiO_2 NMs at 30 °C and 90 °C. Figure 5.8 a and b compares the bare and hydroxylated ZnO NMs at 30 °C. It can be seen that the huge clusters tend to breakdown and NMs arrange more homogenic during the drying process. Figure 5.8 c and d compares the bare and hydroxylated ZnO NMs at 90 °C. Our aim was to investigate combined effect of heating and hydroxylation on the breakdown of clusters,

agglomerates, and arrangement of NMs during the drying process of droplet. It can be seen that the largest cluster of hydroxylated ZnO NMs at 90 °C is about 10 micron and most of the NMs remain in nanometer size.

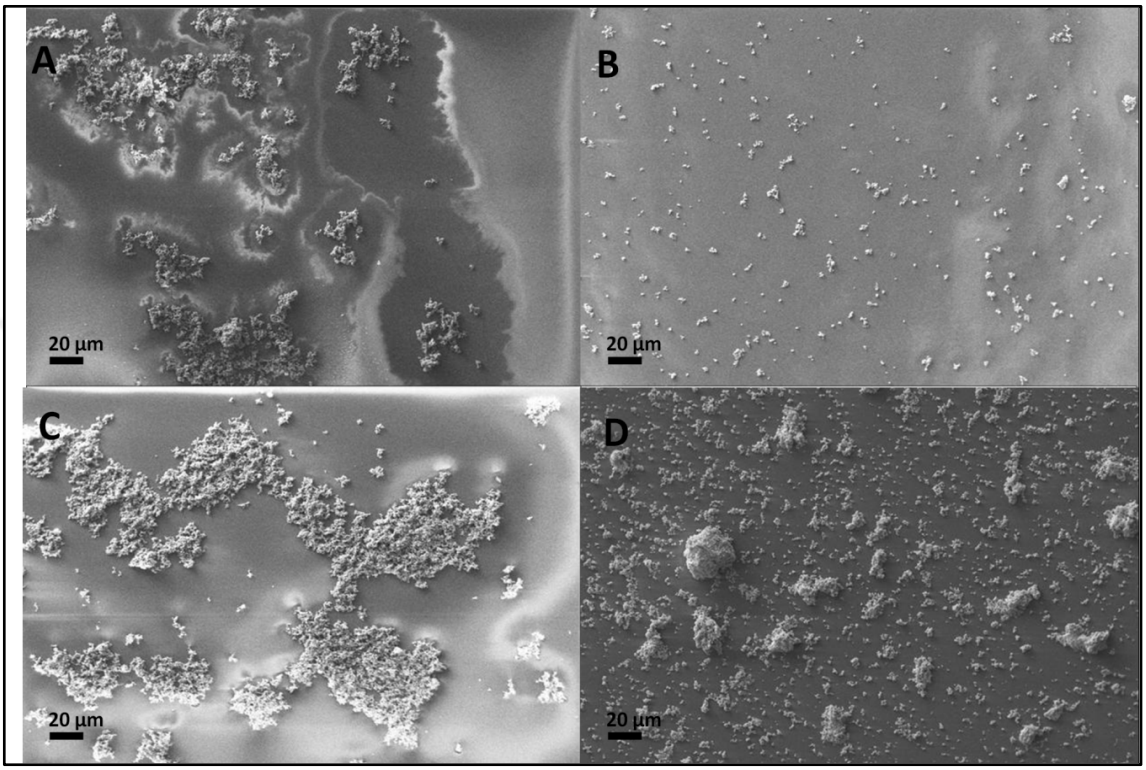

Figure 5.8. SEM images of bare ZnO NMs at 30 °C (A), H_2O_2 treated ZnO NMs at 30 °C (B), bare ZnO NMs at 90 °C (C), H_2O_2 treated ZnO NMs (D)

Figure 5.9 a and b compares the bare and hydroxylated TiO_2 NMs at 30 °C. At 30 °C bare TiO_2 NMs stay as large clusters of 10-50 µm but the hydroxylation breaks down these clusters and results in homogeneous dispersion. In Figure 5.9 c and d, it can be seen the combined effect of hydroxylation and heating on the breakdown of clusters and arrangement of NMs during the drying process of their droplet. Hydroxylated NMs and both heated and hydroxylated NMs do not tend to adhere to each other and form large clusters, they stay in nanometer size and arrange more neatly.

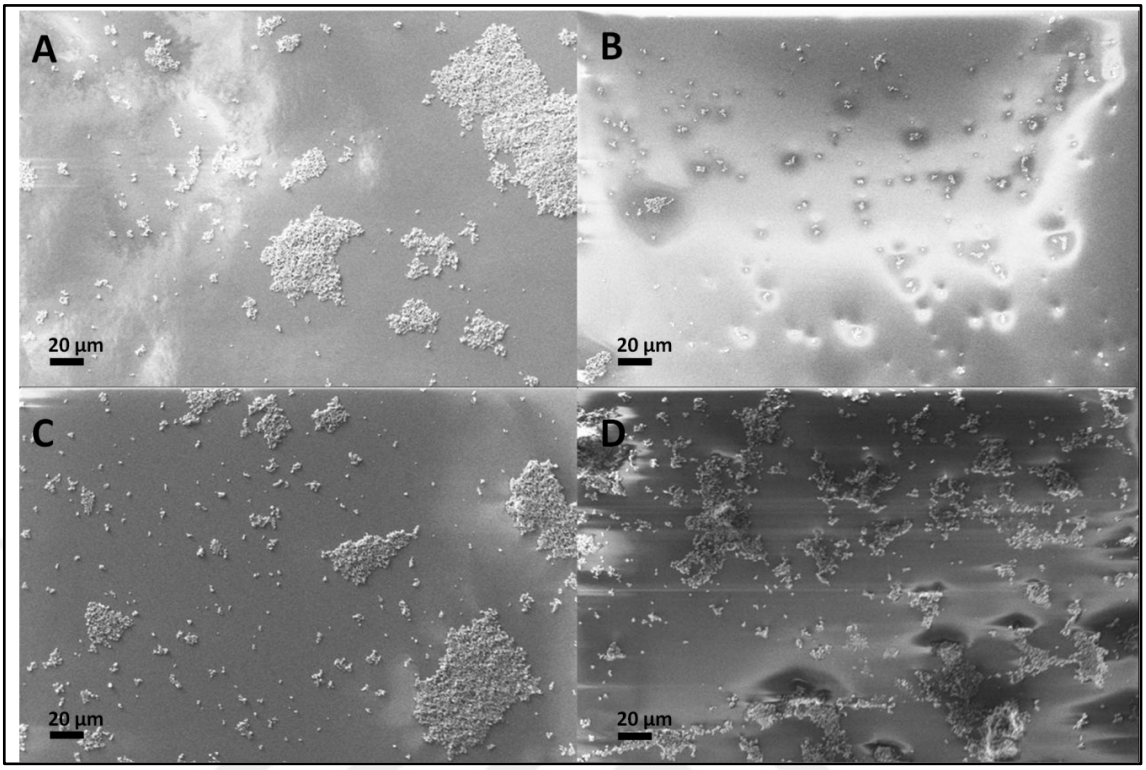

Figure 5.9. SEM images of bare TiO_2 NMs at 30 °C (A), H_2O_2 treated TiO_2 NMs at 30 °C (B), bare TiO_2 NMs at 90 °C (C), H_2O_2 treated TiO_2 NMs (D)

5.3. OLIGONUCLEOTIDE ATTACHMENT ON ZnO and Fe_2O_3 NMs

In this part of the study, the covalent attachment of biomolecules on the surfaces of metal oxide NMs and the validation of their attachment were investigated. The oligonucleotides were attached on NMs by crosslinking process as previously explained. SERS technique was used to investigate the attachment of oligonucleotides on the NMs surface.

In Figure 5.10. the fingerprint bands of adenine and adenine based oligonucleotide (740 cm^{-1}), (1350 cm^{-1}) can be seen. These bands represent the electronic structure of adenine molecule and the bonding between the adenine bases.

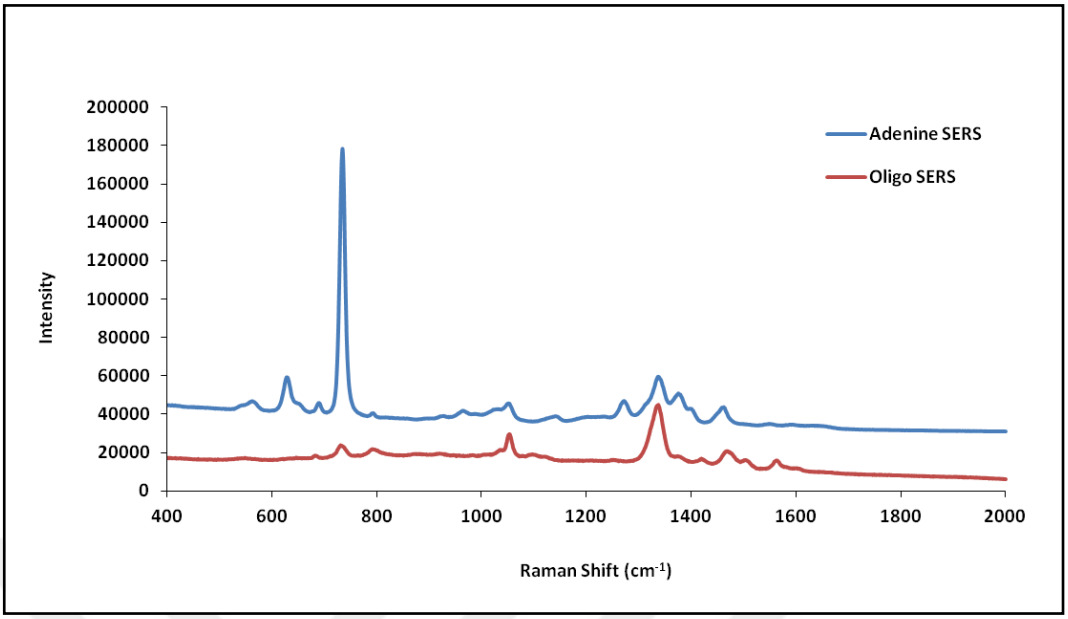

Figure 5.10. SERS spectra of adenine and oligonucleotide

Adenine is a Raman active base which is in the structure of the oligonucleotides used in this study. When adenine gets close vicinity with Ag NMs the signals originating from the ring structure of adenine represses all other low signals and can be observed as high intensity 740 cm $^{-1}$, 1350 cm^{-1} characteristic bands. Thus, oligonucleotides used in this experiment contains 10, 15, 20 or 25 adenine bases in their structure in order to obtain stronger signal from oligonucleotides during Raman measurements.

As described previously, oligonucleotide attached ZnO and Fe_2O_3 NMs were washed 3 times and dialyzed overnight in order to remove any unattached oligonucleotides from NM suspension. As a result, only oligonucleotide attached NM suspension was obtained and 740 cm $^{-1}$, 1350 cm^{-1} characteristic peaks acquired from the SERS measurements performed from NM suspensions directly related with the oligonucleotides on the surfaces of NMs. Thus, SERS can be used as a characterization technique for the attachment of oligonucleotides on the surfaces of NMs.

In Figure 5.11. A, SERS spectra of oligonucleotide attached and bare ZnO NMs can be seen. We can observe the characteristic bands of adenine (740 cm^{-1} and 1350 cm^{-1}) in the Figure. Since the oligonucleotide-ZnO suspension was expected not to contain any free oligonucleotides after the dialysis and washing processes, these bands must be related with

the attached oligonucleotides on the surfaces of ZnO NMs. Different lengths of oligonucleotides were used (10, 15, 20, 25 base long) in order to see the effect of base length in binding efficiency of oligonucleotides. It was observed that especially in ZnO measurements, bands of adenine has higher intensity and sharper bands in the case of 10 base length oligonucleotide attachment. From SERS measurements of oligonucleotide-ZnO NMs, we can say that the oligonucleotides with shorter base length bind to the surfaces of NMs more efficiently.

The influence of gluteraldehyde on the crosslinking process was investigated in order to prove the conjugation of oligonucleotides to the surfaces of NMs undergoes from –OH groups and to eliminate the possibility of random non-covalent attachments. Figure 5.11 A and C. compares the SERS results of oligonucleotide- NM conjugates with gluteraldehyde and without gluteraldehyde. Characteristic bands of oligonucleotides were not observed in oligonucleotide- NM conjugates without gluteraldehyde samples.

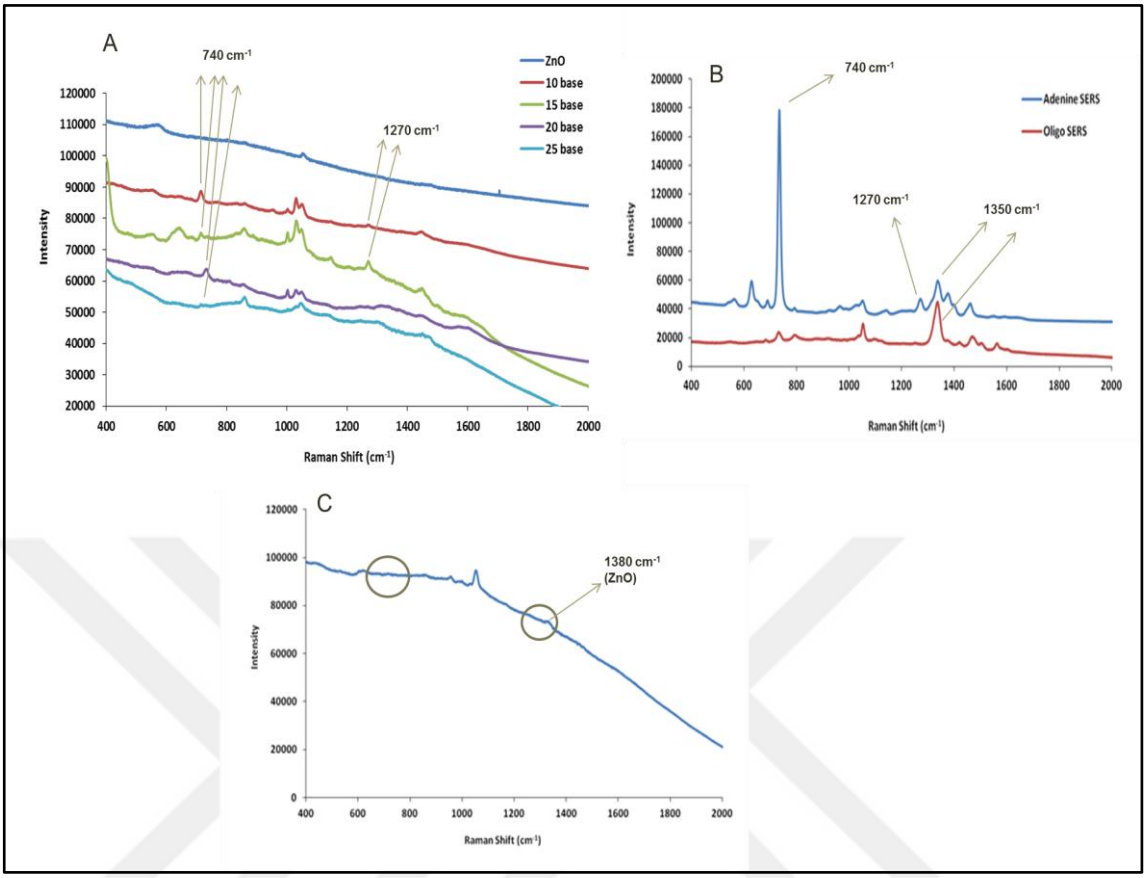

Figure 5.11 SERS spectra of oligonucleotide attached ZnO NMs (A), SERS spectra of adenine and oligonucleotide (B), SERS spectra of ZnO-oligonucleotide mixture without glutaraldeyhde (C).

Figure 5.12. A shows the SERS spectra of bare Fe_2O_3 NMs and oligonucleotide attached Fe_2O_3 NMs. (Different base lengths; 10, 15, 20, 25 base long). The aim was to observe fingerprint bands of adenine from the SERS measurements of oligonucleotide attached Fe_2O_3 NMs since the NM suspensions was not expected to contain any free oligonucleotides any bands related with adenine or oligonucleotides originates from the oligonucleotides attached on the surfaces of Fe_2O_3 NMs. From the Figure 5.12. B, we can observe the characteristic bands of adenine (740 cm^{-1} and 1350 cm^{-1}). When the SERS results of oligonucleotide attached ZnO NMs were compared with the results of oligonucleotide attached Fe_2O_3 NMs, intensities of the bands of adenine (740 cm^{-1} and 1350 cm^{-1}) are higher in ZnO NMs results. Thus, it can be stated that oligonucleotides attach on ZnO NMs surfaces more efficiently than surfaces of Fe_2O_3 NMs.

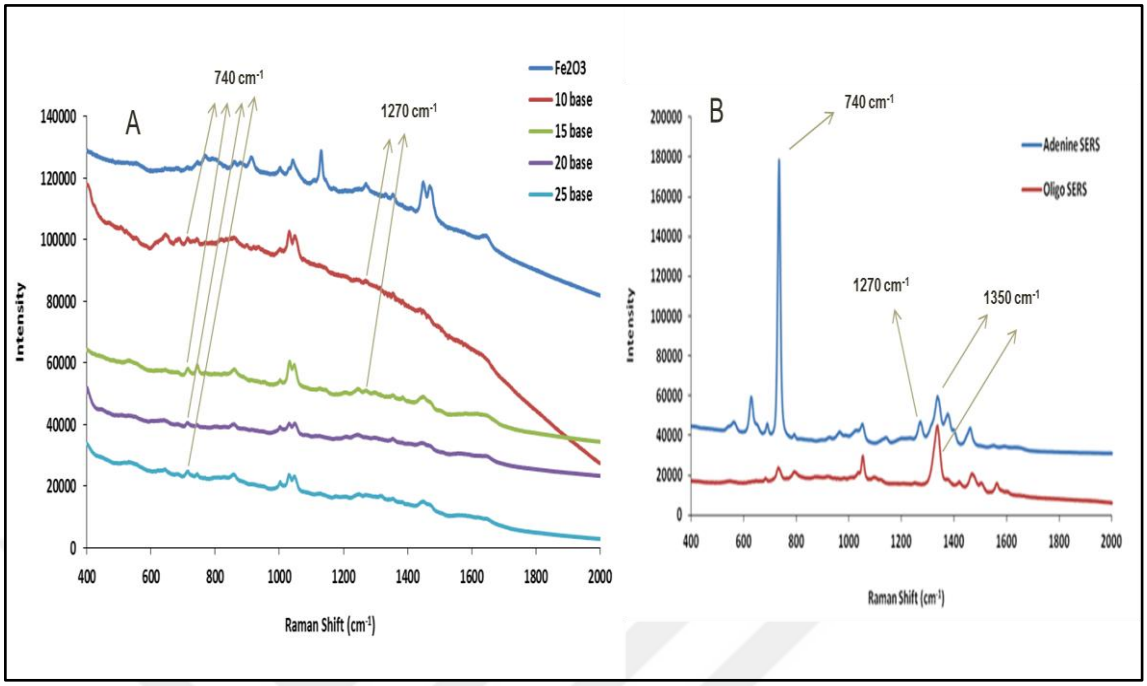

Figure 5.12. SERS spectra of oligonucleotide attached Fe_2O_3 NMs (A), SERS spectra of adenine and oligonucleotide (B)

5.2. INVESTIGATION OF THE PRESENCE OF COATING ON NMs with LASER BREAK DOWN SERS

Starch, chitosan and lactose coated NMs were initially characterized with DLS analysis. Change in the hydrodynamic radius and zeta potential of Fe_2O_3 and TiO_2 NMs was investigated after their surfaces were modified. Figure 5.13 a, b and c shows the change in the size of Fe_2O_3 NMs after surface modification and Figure 5.13 d, e and f shows the change in the size of TiO_2 NMs after surface modification. We can confirm from the DLS results that the hydrodynamic radiuses of the NMs were increased after their surfaces were coated with starch, chitosan and lactose. Only in the case of lactose coated TiO_2 NMs the hydrodynamic size was decreased. It might be explained by the increased dispersion of TiO_2 NMs in dH_2O after their surfaces were coated with lactose.

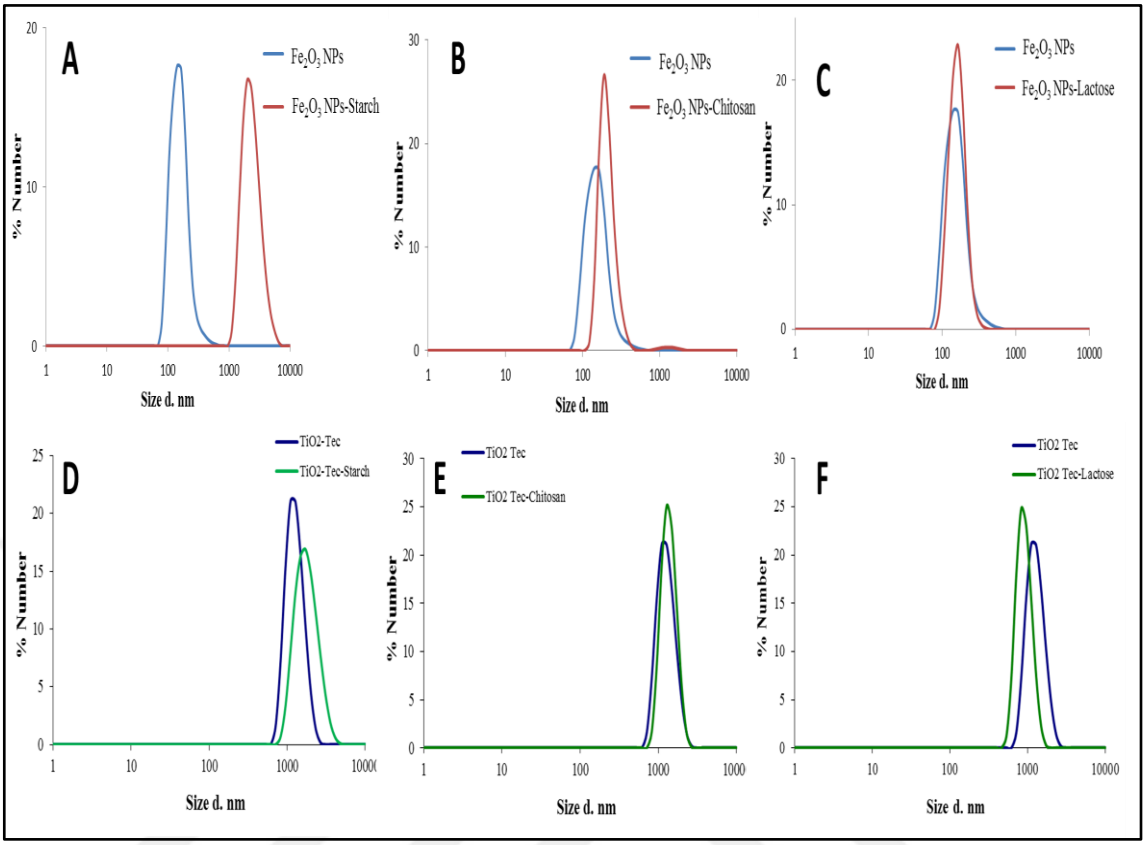

Figure 5.13. Hydrodynamic sizes of starch coated Fe_2O_3 NMs (A), chitosan coated Fe_2O_3 NMs (B), lactose coated Fe_2O_3 NMs (C), starch coated TiO_2 NMs (D), chitosan coated TiO_2 NMs (E) and lactose coated TiO_2 NMs (F)

Zeta potentials of bare and surface modified Fe_2O_3 and TiO_2 NMs can be observed from Table 5.2. Zeta potentials of both Fe_2O_3 and TiO_2 NMs were decreased after their surfaces were coated. Positive shift was observed in the zeta potentials of all surface modified NMs which indicate the alterations in the surface chemistry of NMs.

Table 5.2. Zeta potentials of bare and surface modified NMs

	Bare (mV)	Starch coated(mV)	Chitosan coated(mV)	Lactose coated(mV)
Fe_2O_3 NMs	12.9 ∓ 0.919	15.6 ∓ 0.778	31.8 ∓ 0.707	32.0 ∓ 1.56
TiO_2 NMs	-19.3 ∓ 0.707	-9.6 ∓ 0.184	-9.1 ∓ 0.535	-14.6 ∓ 1.13

Further characterization of coated NMs was performed by FT-IR spectroscopy. Figures 5.14 display the IR spectra of bare and carbohydrate coated Fe_2O_3 and TiO_2 NMs. The FTIR spectra of nanoparticles exhibit broad band at 3300 cm^{-1} due to the –OH groups on NMs surfaces. Increase in the intensity of –OH band at 3300 cm^{-1} supports the statement that the surfaces of NMs were modified with carbohydrates. The –OH groups originating from carbohydrates increases the intensity of broad –OH band. Also, the band at ~2900 cm^{-1} indicates the presence of –CH which exists in carbohydrates in high percentage. From the low frequency region below 1150 cm^{-1}, further information was obtained from the surface attached carbohydrates. From the FT-IR data of modified NMs which was shown in Figure 3, it can be stated that starch, chitosan and lactose was successfully attached on the surfaces of TiO_2 and Fe_2O_3 NMs.

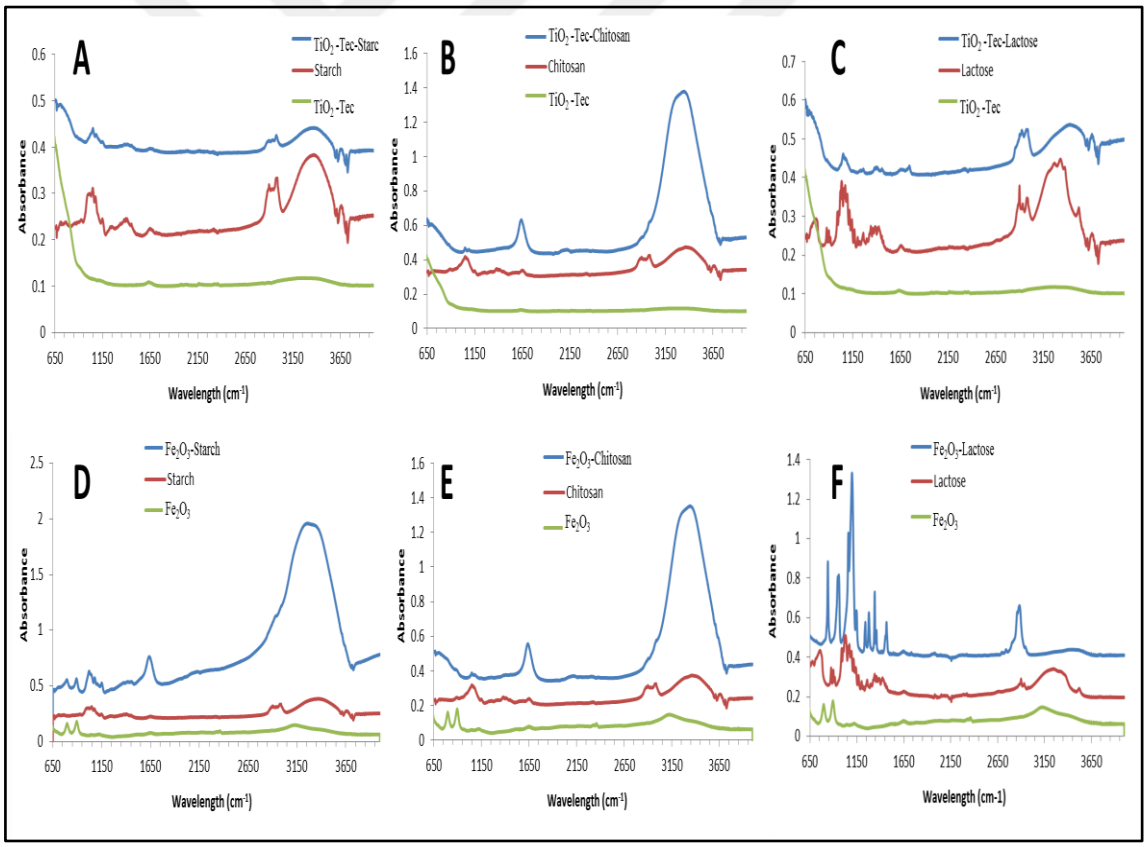

Figure 5.14. FT-IR spectra of starch coated TiO_2 NMs (A), chitosan coated TiO_2 NMs (B), lactose coated TiO_2 NMs (C), starch coated Fe_2O_3 NMs (D), chitosan coated Fe_2O_3 NMs (E) and lactose coated Fe_2O_3 NMs (F)

The laser wavelength used in the experiment is the visible region of the spectrum and highly energetic. The biomolecular structures exposed to such a laser light at prolonged exposure should degrade. The basis of the idea is a well-known decomposition phenomenon observed in Raman spectroscopy and SERS experiments [86, 87]. The carbohydrates are chosen as surface coating materials for the experiments since they are difficult to characterize on the NMs. The starch, chitosan, and lactose are chemically bound to the MONP surface though glutaraldehyde linkage. In such case, there should be thicker starch or chitosan layer on the NM surface than lactose since starch or chitosan are polymeric structures. Our aim was to observe any possible changes in the spectrum of coated NMs while they melt down due to the high laser power. Elevated cycles of laser power exposure results in the degradation of biological samples such as carbohydrates or chitosan. Thus, chemically attached lactose, chitosan and starch molecules on the surfaces of NMs can be degraded by exposing to laser power. As a result of degradation, larger particles such as chitosan and starch start to melt down and lose their original shape on the surfaces of NMs. These large molecules cover the surfaces of NMs as a thick layer after their melt down. Small molecules like lactose also melt down due to the exposure of laser power, but it cannot form thick layers on the surfaces of NMs due to its small size. As a result of the formation of this thick layer around the NMs Raman signal of the NMs weakens. As the materials on the surface melt down and form thicker layers Raman signal coming from the core NMs was expected to decrease. Fig. 5.15 shows the change in the spectrum of starch, chitosan and lactose coated TiO_2 NMs. By comparing the change in bare TiO_2 NMs (A) with starch chitosan and lactose coated TiO_2 NMs it can be observed that the melt down of surface coatings has a negative influence on the bands at 100 cm^{-1}, 480 cm^{-1},550 cm^{-1} and 620 cm^{-1}. Since these bands are related with the bare TiO_2 NMs our theory was supported and we demonstrated evidences of surface coatings on TiO_2 NMs. Figure 5.15 A and D has similar spectra and intensity change was not observed because of the lack of formation of layers after melt down of lactose. However, in fig. 5.15 B and C same level of decrease in the intensities due to the formation of layers on the surfaces of TiO_2 NMs result of the melt down of coatings.

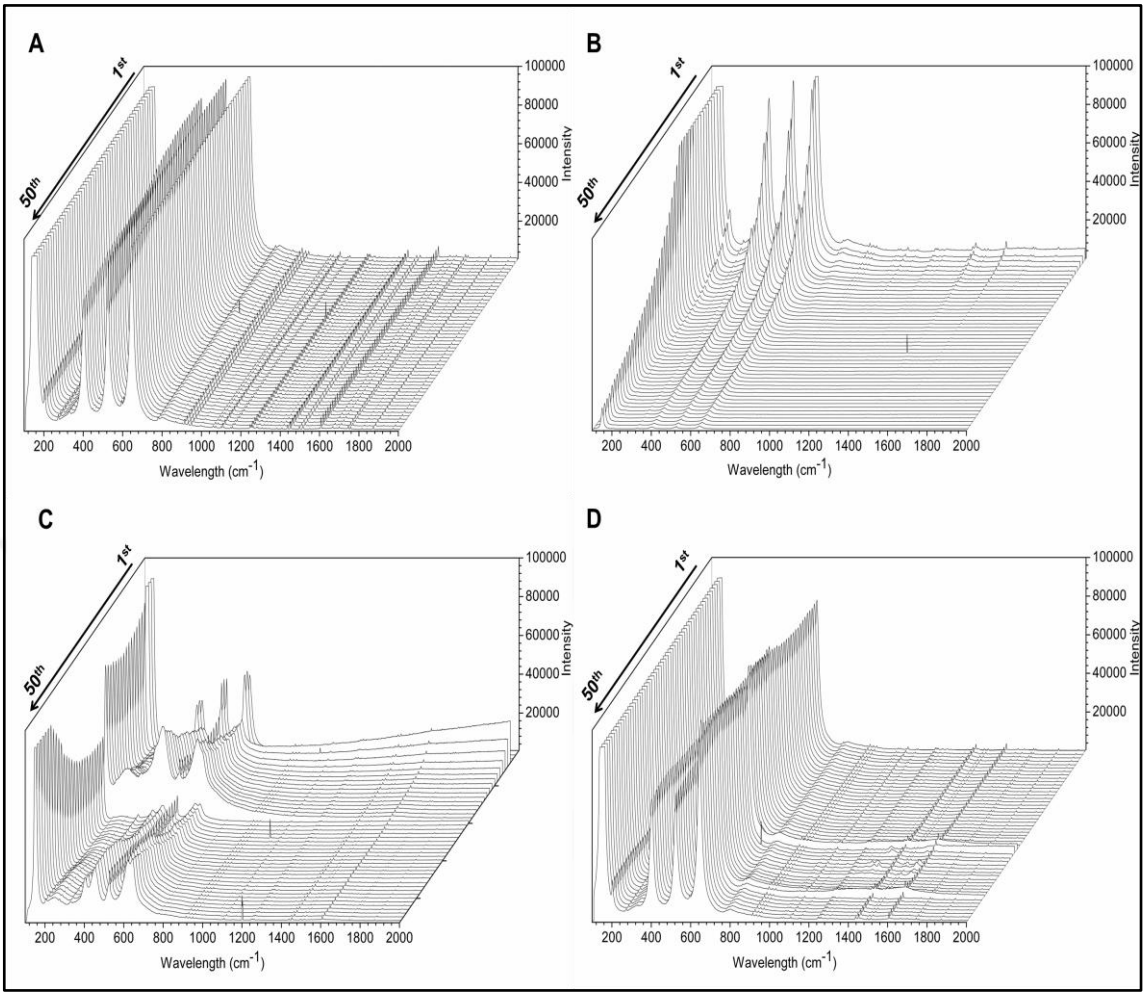

Figure 5.15. Raman spectrum of Bare TiO_2 (A) Starch coated TiO_2 (B) Chitosan coated TiO_2 (C) and Lactose coated TiO_2 (D) after laser power exposure

Figure 5.16 shows the change in the spectrum of starch, chitosan and lactose coated Fe_2O_3 NMs after exposure to laser power. It was observed that the intensities of the characteristic bands of bare Fe_2O_3 NMs did not change after exposure to laser power. Bands at 280 cm^{-1}, 300 cm^{-1}, 400 cm^{-1}, 490 cm^{-1}, 600 cm^{-1} and 1310 cm^{-1} which are characteristic bands of bare Fe_2O_3 NMs were observed for possible changes in their intensities. From the fig 5.16 B and C it was observed that especially the intensity of 1310 cm^{-1} band decreases dramatically. No change in the intensities of any of the characteristic bands were observed in fig 5.16 D, lactose coated Fe_2O_3 NMs. Again this situation can be explained by the formation of thick layers on the surfaces of Fe_2O_3 NMs due to melt down of surface materials. Formation of thick layer was observed on the surfaces of starch and chitosan coated Fe_2O_3 NMs after exposure to laser power. 1600 cm^{-1} band was only observed at

chitosan coated Fe_2O_3 NMs and it vanishes rapidly after laser power exposure. We assume that it originates from glutaraldehyde but further investigation is needed to understand the reason for observing this band only at chitosan coated NMs.

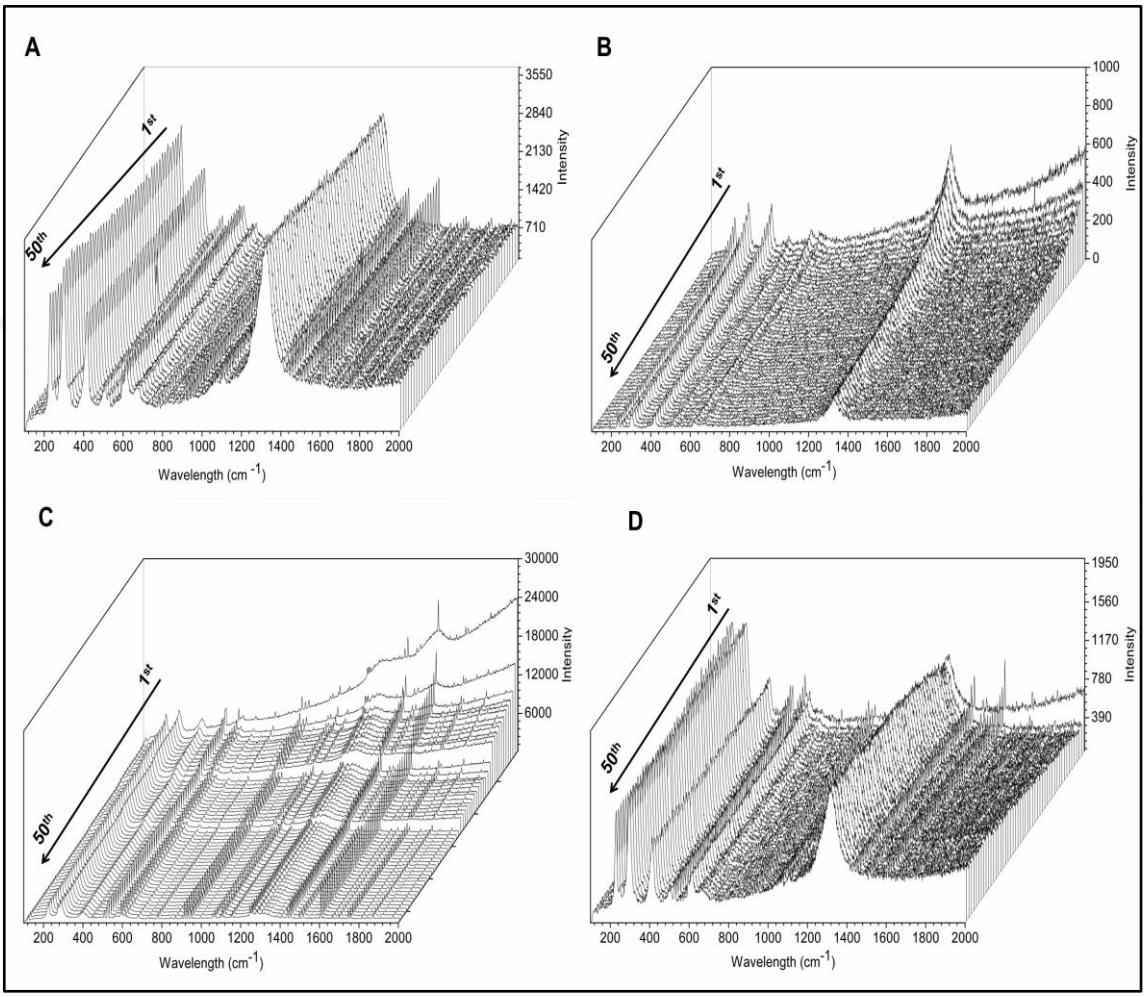

Figure 5.16. Raman spectrum of Bare Fe_2O_3 (A) Starch coated Fe_2O_3 (B) Chitosan coated Fe_2O_3 (C) and Lactose coated Fe_2O_3 (D) after laser power exposure

SERS provides an enhancement on the spectra of biological samples when molecule of interest was brought in close contact with a noble metal such as gold and silver. The enhancement on the spectra may allow the observation of the bands that cannot be observed with Raman spectroscopy. Therefore, chitosan coated TiO_2 and Fe_2O_3 NMs were mixed with Ag NPs and exposed to laser power. Modified NMs were mixed with concentrated (8x) Ag NPs and prepared mixture was dropped on CaF_2 slides. The samples were dried in suspended form. Figure 5.17 shows the SERS spectrum of chitosan coated

TiO_2 and Fe_2O_3 NMs. Chitosan coated NMs were chosen for SERS experiments because of the successful formation of layers after its melt down and the most significant change in the spectrum was observed from chitosan and starch coated NMs by Raman spectroscopy.

SERS measurements also proved that the chitosan starts to melt down and forms a layer around the NMs after laser power exposure. The intensities of the characteristic bands of NMs decrease and even lost. As it was observed from Fig 5.17 A and B, 1600 cm^{-1} band was again observed in each SERS measurements. Its intensity decreased and the peak was lost after the exposure of laser power. 1600 cm^{-1} band might be related with the presence of glutaraldehyde but further investigation is needed to make more certain statements.

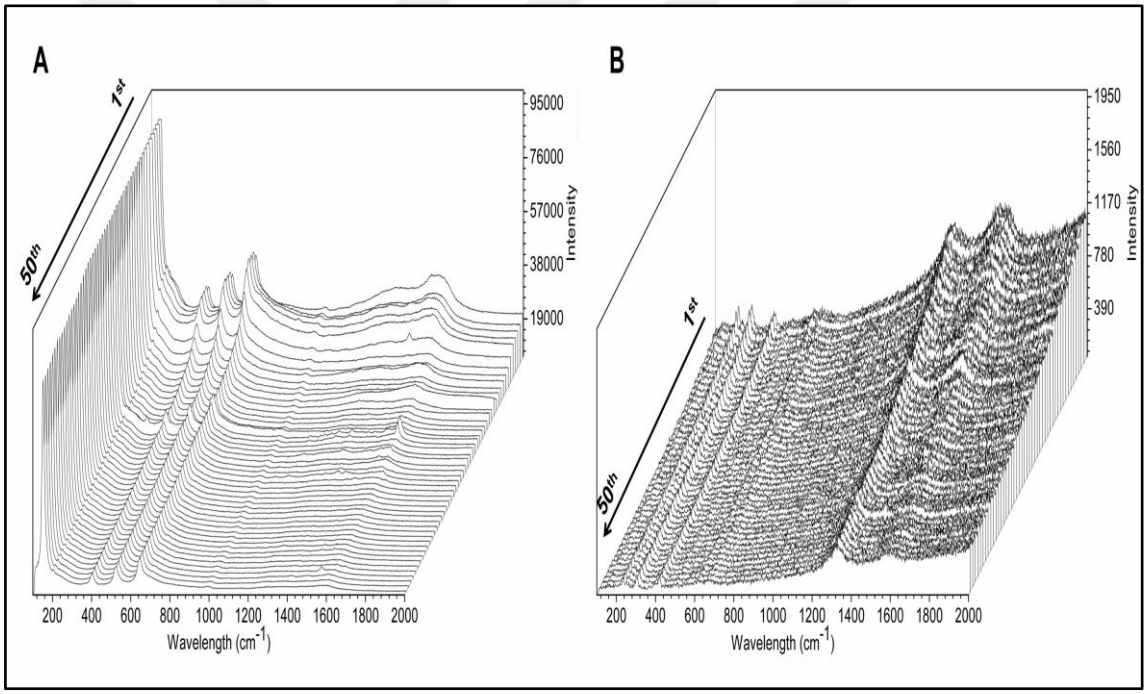

Figure 5.17. SERS spectra of chitosan coated TiO_2 (A), Fe_2O_3 (B) NMs after laser exposure

6. CONCLUSION AND RECOMMENDATIONS

6.1. CONCLUSION

The surface modification of NMs is an important step for the alteration of their behaviors to provide further benefit from their unique properties in variety of applications. In this thesis, the surface modifications of MONMs such as ZnO, TiO_2 and Fe_2O_3 with biomolecules such as oligonucleotides and carbohydrates are investigated.

In the first part of the study, we aimed to overcome the agglomeration problem of NMs in aqueous environments. For this purpose, ZnO and TiO_2 NMs were treated with hydrogen peroxide. Hydrogen peroxide treatment washes the surfaces of NMs and the inserts –OH groups onto the surfaces of them. After hydrogen peroxide treatment process, hydroxylated NMs gained higher dispersion in aqueous environments when compared to their bare forms. Hence, the effect of heating on the size distribution of hydrogen peroxide treated NMs were investigated. During our study results showed that, combined effect of heating and hydroxylation decreased on the size of the NMs. This method can be a solution for the lack of dispersion of NMs in aqueous environments.

In the second part of the study, we investigated a new approach to attach oligonucleotides onto the NMs by using glutaraldehyde which crosslinks two free –OH groups and characterized by SERS. From the SERS spectra of oligonucleotide attached NMs 740 cm^{-1} and 1350 cm^{-1} peaks were investigated. Free oligonucleotides were washed and dialyzed from the NM suspension, so 740 cm^{-1} and 1350 cm^{-1} peaks can only be originated from the surface attached oligonucleotides. Thus, SERS can be used as a characterization technique for the attachment of oligonucleotides on the surfaces of NMs.

In order to confirm the attachment of starch, chitosan and lactose to the NMs, Raman spectroscopy and SERS was used. In this part of the study, we aimed to melt down the coated materials by using laser power originating from the Raman spectroscopy system. On the same spot 514 nm laser power was exposed for 20 s with 50 spectral collections and spectrum was acquired after each exposure. When the spectra were analyzed

intensities of the characteristic bands of NMs were decreased and even disappeared. As a result of the melt down of coating materials, large particles such as chitosan and starch melt down and lose their original shape on the surfaces of the NMs. These large molecules cover the surfaces of NMs as a layer as they melt down with heating. However, a small molecule like lactose cannot form thick layers on the surfaces of NMs due to their small size. As a result of the formation of this layer, Raman signal of the NMs weakens. As the materials on the surface melt down and form thicker layers the intensity of the characteristic bands of NMs decreases. It is also possible that the melted coating may mobilize the NMs and the NMs may escape from the laser spot, resulting the decrease of the NMs under the laser spot and dependently resulting in the intensity of the bands originating from the NMs. After the Raman measurements, SERS measurements were carried out to observe some characteristic peaks of coating materials and disappearance of those peaks after the melt down. In all SERS measurements, the band at 1590 cm^{-1} disappeared for all chitosan coated NMs. Although the 1590 cm^{-1} band is not characteristic for any of the NMs, used in our study, the formation and following disappearance of the band can be related with gluteraldehyde. Also the intensities of the characteristic peaks of NMs decreased in SERS experiments too.

6.2. RECOMMANDATIONS

Hydroxylation of NMs can increase the dispersion of NMs in aqueous environments as it was demonstrated. This approach may allow the dispersion of metal oxides without their contamination. Although the study demonstrates that the use of H_2O_2 improves the dispersion of agglomerated metal oxides, it is suggested that the approach should be tested for different metal oxide NMs to evaluate if the H_2O_2 treatment is specifically valid for certain type of MONMs or not. In addition, the mechanism that how H_2O_2 acts on the NM surfaces, is not clear and this should be investigated in more systematic way.

As novel approaches, the use of Raman spectroscopy and SERS were used to confirm the biomolecules onto the MONM surface. The results obtained from the study are very promising and the approach should be further investigated using different types of biomacromolecules. A more systematic study using mono-, di-, tri-, oligo, and poly saccharides can be undertaken to investigate the influence of the molecule size on the

approach. Then, the study can be expanded to cytotoxicity testing whether the attached molecules are effectively providing biological protection for living systems.

REFERENCES

1. Taniguchi, N., "On the Basic Concept of 'Nano-Technology'". *Proceedings of the International Conference on Production Engineering*, Part II, Tokyo, 1974.

2. "The Scale of Things - Nanometers and More", Online simulation and more for nanotechnology, https://nanohub.org/resources/13842, 2012.

3. Kazuyuki, U., O. Susumu, S. Kenji, and O. Atsushi, "Quantum effects in a cylindrical carbon-nanotube Capacitor" , *Journal of Physics.: Condensed. Matter* , Vol.19, pp.7, 2007.

4. Parka, J. B., J. Graciania, J. Evans, D. Stacchiolaa, S. Maa, P. Liua, A. Nambua, J. F. Sanzc, J. Hrbeka and J. A. Rodrigueza, "High catalytic activity of Au/CeOx/TiO_2(110) controlled by the nature of the mixed-metal oxide at the nanometer level", *Proceedings of the national academy of sciences of the United States of America,* Vol.106, pp.4975-4980, 2009.

5. Caminale, M., L. Anghinolfi, E. Magnano, F. Bondino, M. Canepa, L. Mattera, F. Bisio, "Tuning the Magneto-optical Response of Iron Oxide Nanocrystals in Au- and Ag-Based Plasmonic Media", *ACS Applied Materials and Interfaces,* Vol.5 pp.1955-1960, 2013.

6. Han, A. R., T. W. Kim, D. H. Park, S. J. Hwang, J. H. Choy, "Soft chemical dehydration route to carbon coating of metal oxides: Its application for spinel lithium manganate", *Journal of Physical Chemistry C* , Vol.111, pp.11347-11352, 2007.

7. Gallo, J., I. Garcia, D. Padro, B. Arnaiz, S. Penades, "Water-soluble magnetic glyconanoparticles based on metal-doped ferrites coated with gold: Synthesis and characterization", *Journal of Material Chemistry,* Vol.20, pp.10010-10020, 2010.

8. Fuente, D. L., M. Jesus, D. Alcantara, P. Eaton, "Gold and gold-iron oxide magnetic glyconanoparticles: Synthesis, characterization and magnetic properties", *The Journal of Physical Chemistry B*, Vol.110, pp.13021-13028, 2006.

9. Ma, D., S. E. Bettis, K. Hanson, M. Minakova, L. Alibabaei, W. Fondrie, D. M. Ryan, G. A. Papoian, T. J. Meyer, M. L. Waters, J. M. Papanikolas, "Interfacial Energy Conversion in Ru-II Polypyridyl-Derivatized Oligoproline Assemblies on TiO_2", *Journal of The American Chemical Society*, Vol.135, pp.5250-5253, 2013.

10. Ebrahimi, S., T. K. Ghafoori, T. H. Rafii, "Molecular dynamics simulation of the adhesive behavior of collagen on smooth and randomly rough TiO_2 and Al2O3 surfaces" *Computational Materials Science*, Vol.71, pp.172-178, 2013.

11. Cha, T.G., B. A. Baker, J. Salgado, C. J. Bates, K. H. Chen, A. C. Chang, M. C. Akatay, J. H. Han, M. S. Strano, J. H. Choi, "Understanding Oligonucleotide-Templated Nanocrystals: Growth Mechanisms and Surface Properties", *ACS Nano*, Vol.6, pp.8136-8143, 2012.

12. Weng, C.J., Y. L. Chen, Y. S. Jhuo, Y. L. Lin, J. M. Yeh, "Advanced antistatic/anticorrosion coatings prepared from polystyrene composites incorporating dodecylbenzenesulfonic acid-doped SiO2 polyaniline coreshell microspheres", *Polymer International*, Vol.62, pp.774-782, 2013.

13. Taheri, P., J. R. Flores, F. Hannour, J. H. W. de Wit, H. Terryn, J. M. C. Mol, "In Situ Study of Buried Interfacial Bonding Mechanisms of Carboxylic Polymers on Zn Surfaces", *Journal of Physical Chemistry C*, Vol.117, pp.3374-3382, 2013.

14. Fei, L., M. Naeemi, G. F. Zou, H. M. Luo, "Chemical Solution Deposition of Epitaxial Metal-Oxide Nanocomposite Thin Films", *Chemical Record*, Vol.13, pp.85-101, 2013.

15. Sun, C., J. S. H. Lee, M. Zhang, "Magnetic nanoparticles in MR imaging and drug delivery", *Advanced Drug Delivery Reviews*, Vol.60, pp.1252-1265, 2008.

16. Prutton M., Introduction to Surface Physics, Oxford Science Publications, Oxford, 1994.

17. Ayyub, P., V. R. Palkar, S. Chattopadhyay, M. Multani, "Effect of crystal size reduction on lattice symmetry and cooperative properties", *Physical Review B*, Vol.51, pp.6135-6138, 1995.

18. Cammarata, R.C., K. Sieradki, "Effects of surface stress on the elastic moduli of thin films and superlattices", *Physical Review. Letter*., Vol.62, pp. 2005, 1989.

19. Yoffre, A. D., "Low-dimensional systems: quantum size effects and electronic properties of semiconductor microcrystallites (zero-dimensional systems) and some quasi-two-dimensional systems" *Advances in Physics*, Vol.42, pp. 173-266, 1993.

20. Brus, L., "Electronic wave-functions in semiconductor clusters - experiment and theory" *J. Phys. Chem.* Vol.90, pp. 2555-2560, 1986.

21. Fernández-García, M., J. C. Conesa, F. Illas, "Effect of the Madelung potential value and symmetry on the adsorption properties of adsorbate/oxide systems" *Surface Science.*, Vol. 339, pp. 207-215, 1996.

22. Hoffmann, R., Solids and Surfaces: A Chemist's View of Bonding in Extended Structures; VCH, New York, 1988.

23. Kung, H.H. Transition Metal Oxides: Surface Chemistry and Catalysis; Elsevier: Amsterdam, 1989.

24. Rodríguez, J.A., M. Fernández-García, Synthesis, Properties and Applications of Oxide Nanoparticles, Whiley, New Jersey, 2007.

25. Fernández-García, M., A. Martínez-Arias, J. C. Hanson, J. A. Rodríguez, "Nanostructured Oxides in Chemistry: Characterization and Properties" *Chemistry Review* Vol.104, pp.4063-4104, 2004.

26. Henrich V.E., P. A. Cox, “The Surface Chemistry of Metal Oxides” Cambridge University Press, Cambridge, UK, 1994.

27. Hoffmann, M.R., S. T. Martin,, W. Choi, and D. W. Bahnemann, , ‘‘Environmental Applications of Semiconductor Photocatalysis’’, *Chemistry Rev*iew, Vol. 95, pp. 69-96, 1995.

28. Kamat, P.V., “Photochemistry on nonreactive and reactive (semiconductor) surfaces” *Chemistry Review*, Vol.93, pp.267, 1993.

29. Livage, J., M. Henry, C. Sanchez, “Sol-gel chemistry of transition metal oxides” *Progress in Solid State Chemistry,* Vol.18, pp. 259–341, 1988.

30. Tjong, S.C., H. Chen, “Nanocrystalline materials and coatings*” Material Science Eng*ineering, Vol. 45, pp.1-88, 2004.

31. Hao, R., R. J. Xing, Z. C. Xu, Y. L. Hou, S. Gao, S. H. Sun, “Synthesis, Functionalization, and Biomedical Applications of Multifunctional Magnetic Nanoparticles”, *Advanced Materials*, Vol.22, pp.2729-2742, 2010.

32. Bae, K.H., K. Lee, C. Kim, T. G. Park, “Surface functionalized hollow manganese oxide nanoparticles for cancer targeted siRNA delivery and magnetic resonance imaging” *Biomaterials*, Vol.32, pp.176-184, 2011.

33. Luo, X. L., A. Morrin, A. J. Killard, M. R. Smyth, “Application of nanoparticles in electrochemical sensors and biosensors”, *Electroanalysis*, Vol.18, pp.319-326, 2006.

34. Hoffmann, M. R., S. T. Martin, W. Choi, D. W. Bahnemann, ‘‘Environmental Applications of Semiconductor Photocatalysis’’, *Chemistry Review*, Vol.95, pp.69-96, 1995.

35. Choi S. U. S., Z. G. Zhang, F. E. Lockwood, E. A. Grulke, "Anomalous thermal conductivity enhancement in nanotube suspensions", *Applied Phyics Letters*, Vol.79, pp.2252–2254, 2001.

36. Fernández-García, M., A. Martínez-Arias, J. C. Hanson, J. A. Rodríguez, "Nanostructured Oxides in Chemistry: Characterization and Properties", *Chemistry Review*, Vol.104, pp.4063-4104, 2004.

37. Tang, E. J., H. Liu, L. M. Sun, E. L. Zheng, G. X. Cheng, "Fabrication of zinc oxide/poly(styrene) grafted nanocomposite latex and its dispersion", *European Polymer Journal*, Vol.43, pp.4210-4218, 2007.

38. Hong, R. Y., J. Z. Qian, J. X. Cao, "Synthesis and characterization of PMMA grafted ZnO nanoparticles" *Powder Technology*, Vol.163, pp.160-168, 2006.

39. Dange, C., T. N. T. Phan, V. Andre, J. Rieger, J. Persello, A. Foissy, "Adsorption mechanism and dispersion efficiency of three anionic additives [poly(acrylic acid), poly(styrene sulfonate) and HEDP] on zinc oxide" *Journal of Colloids and Interfaces Science*, Vol.315, pp.107-115, 2007.

40. Kole, M., T. K. Dey, "Effect of prolonged ultrasonication on the thermal conductivity of ZnO–ethylene glycol nanofluids", *Thermochimica Acta*, Vol.535, pp.58–65, 2012.

41. Neppiras, E. A., "Acoustic cavitation", *Physics Report*, Vol.61, pp.159–251, 1980.

42. Kusters, K. A., S. E. Pratsinis, S. G. Thoma, D. M. Smith, "Ultrasonic fragmentation of agglomerate powders", *Chemical Engineering Science*, Vol.48, pp.4119–4127, 1993.

43. Aoki, M., T. A. Ring, J. S. Haggerty, "Analysis and modeling of the ultrasonic dispersion technique", *Advanced Ceramic Materials*, Vol.2, pp.209–212, 1987.

44. Peck, A. W., P. Ding, A. T. Utomo, “Effect of energy density, pH and temperature on deaggregation in nano-particles-water suspensions in high shear mixer”, *Powder Technology*, Vol.173, pp.203–210, 2007.

45. Mandzy, N., E. Grulke, T. Druffel, “Breakage of TiO_2 agglomerates in electrostatically stabilized aqueous dispersions”, *Powder Technology*, Vol.160, pp.212-126, 2005.

46. Udbhav, O., D. Sumitesh, C. Subhrakanti, “Stability, pH and Viscosity Relationships in Zinc Oxide Based Nanofluids Subject to Heating and Cooling Cycles”, *Material Science Engineering*, Vol.4, pp.24-29, 2010.

47. Duangthongsuk, W., S. Wongwises, “Measurement of temperature-dependent thermal conductivity and viscosity of TiO_2–water nanofluids”, *Experimental Thermal and Fluid Science*, Vol.33, pp.706–714, 2009.

48. Lee, S. W., S. D. Park, S. Kang, I. C. Bang, J. H. Kim, “Investigation of viscosity and thermal conductivity of SiC nanofluids for heat transfer applications”, *International Journal of Heat and Mass Transfer*, Vol.54, pp.433–438, 2011.

49. Longo, G. A., C. Zilio, “Experimental measurement of thermophysical properties of oxide–water nano-fluids down to ice-point”, *Experimental Thermal and Fluid Science*, Vol.35, pp.1313–1324, 2011.

50. Doty, R.C., T. R. Tshikhudo, M. Brust, D. G. Fernig, “Extremely Stable, Water-Soluble, Ag Nanoparticles”, *Chemistry of Materials*, Vol. 17, pp. 4630-4635, 2005.

51. Pukanszky, B., E. Fekete, "Adhesion and surface modification", *Advanced Polymer Science*, Vol.139, pp. 109-153, 1999.

52. Kickelbick, G., U. Schubert, “Organic functionalization of metal oxide nanoparticles”, in M. I. Baraton (eds), *Synthesis, Functionalization and Surface Treatment of Nanoparticles*., pp. 91, Stevenson Ranch, France, 2003.

53. Templeton, A. C., W. P. Wuelfing, R. W. Murray, "Monolayer-protected cluster molecules", *Accounts of Chemical Research*, Vol.33, pp.27–36, 2000.

54. Hostetler, M. J., J. E. Wingate, C. J. Zhong, J. E. Harris, R. W. Vachet, M. R. Clark, J. D. Londono, S. J. Green, J. J. Stokes, G. D. Wignall, G. L. Glish, M. D. Porter, N. D. Evans, R. W. Murray, "Alkanethiolate Gold Cluster Molecules with Core Diameters from 1.5 to 5.2 nm: Core and Monolayer Properties as a Function of Core Size'', *Langmuir*, Vol. 14, pp. 17-30, 1998.

55. Sun, Y.P., K. Fu, Y. Lin, W. Huang, "Functionalized carbon nanotubes: Properties and applications", *Accounts of Chemical Research*, Vol.35, pp.1096-1104, 2002.

56. Warner, M. G., J. E. Hutchison, ''Synthesis, Functionalization and Surface Treatment of Nanoparticles'', in M. I. Baraton, R. Stevenson (eds), *Synthesis and assembly of functionalized gold nanoparticles*, pp. 672003, USA, 2002.

57. Jiang, H., K. S. Moon, Y. Li, C. P. Wong, ''Surface functionalized silver nanoparticles for ultra-highly conductive polymer composites'', *Chemistry of Materials*, Vol. 18, pp. 2969-2973, 2006.

58. Fadeev, A. Y., Y. V. Kazakevich, ''Covalently Attached Monolayers of Oligo(dimethylsiloxane)s on Silica: A Siloxane Chemistry Approach for Surface Modification'', *Langmuir*, Vol. 18, pp. 2665- 2672, 2002.

59. Wu, C. G., L. F. Tzeng, Y. T. Kuo., C. H. Shu, "Enhancement of the photocatalytic activity of TiO_2 film via surface modification of the substrate" *Applied Catalysis A*, Vol.226, pp.199-211, 2002.

60. Hermanson, G. T., ''Bioconjugate Techniques'', California: Academic press, San Diego, 1996.

61. De La Fuente, J. M., D. Alcantara, S. Penades, ‘‘Cell response to magnetic glyconanoparticles: does the carbohydrate matter?’’, *IEEE Transection on Nanobioscience*, Vol.6, pp.275- 281, 2007.

62. Smith, A. M., ‘‘The biosynthesis of starch granules’’, *Biomacromolecules*, Vol. 2, pp.335–341, 2001.

63. Seetharaman, K., and E. Bertoft, “Differences in structures of starch hydrolysates using saliva from different individuals”, *Starch – Stärke*, Vol.65, pp.1–7, 2013.

64. John, F., R. Mukerjea, “Evolution of the development of how starch is biosynthesized”, *Starch – Stärke,* Vol.65, pp.8-21, 2013.

65. Borchard, G., ‘‘Chitosan in gene delivery", *Advanced Drug Delivery Review*, Vol. 52, pp. 145–150, 2001.

66. Corsi, K, F. Chellat, L. Yahia, J. C. Fernandes, ‘‘Mesenchymal stem cells, MG63 and HEK293 transfection using chitosan-DNA nanoparticles’’, *Biomaterials*, Vol.24, pp.1255-1264, 2003.

67. Tsigos, L., A. Martinou, D. Kafetzopoulos, and V. Bouriotis, ‘‘Chitin deacetylases: new, versatile tools in biotechnology’’, *Trends in Biotechnology,* Vol.18, pp.305-312, 2000.

68. Krajewska, B., ‘‘Application of chitin- and chitosan based materials for enzyme immobilizations: a review’’, *Enzyme and Microbial Technology*, Vol.35, pp.126-139, 2004.

69. Roh, I. J., and I. C. J. Kwon, “Fabrication of a pure porous chitosan bead matrix: influences of phase separation on the microstructure”, *Biomaterial Science,* Vol.13, pp.769-782, 2002.

70. Kim, S. B., Y. J. Kim, T. L. Yoon, S. A. Park, I. H. Cho, E. J. Kim, I. A. Kim, J. W. Shin, ‘‘The characteristics of a hydroxyapatite–chitosan–PMMA bone cement’’, *Biomaterials*, Vol.25, pp.5715-5723, 2004.

71. Wang, J., J. de Boer, K. J. de Groot, ‘‘Preperation and properties of electrodeposited calcium phosphate/chitosan coatings’’, *Journal of Dental Research*, Vol.83, pp.296-301, 2004.

72. Holme, D. J., H. Peck, *Analytical Biochemistry*, , 3rd edition, Princtice Hall, pp.36, 1998.

73. Kumar, U. S., “Surface-Enhanced Raman Spectroscopy Recent Advancement of Raman Spectroscopy”, *Resonance*, Vol.15, pp.154-164, 2010.

74. Kelf, T., ‘‘Surface Enhanced Raman Spectroscopy’’, 2012 http://www.timkelf.com/Research/ResearchSERS.html, (retrieved January 2012).

75. Raman, C. V., K. S. Krishnan, “A New Type of Secondary Radiation”, *Nature*, Vol.121, pp.501-502, 1928.

76. Landsberg and Mandelstam, ‘‘Über die Lichtzerstreuung in Kristallen’’, *Zeitschrift für Physik*, Vol.50, pp.769-780, 1928.

77. Moskovits, M., D. P. Dillella, ‘‘Surface Enhanced Raman Scattering’’, In R. K. Chang, T. E. Furtak, (eds), *Spectroelectrochemistry: Theory and Practice*., USA: Plenum Press, New York, pp .243–273, 1982.

78. Moskovits, M., ‘‘Surface-enhanced spectroscopy’’, *Reviews of Modern Phys*ics, Vol.57, pp.783-826, 1985.

79. Kahraman, M., M. Yazici, , F. Sahin, , O. F. Bayrak, , M. Culha, “Reproducible Surface-Enhanced Raman Scattering Spectra of Bacteria on Aggregated Silver Nanoparticles”, *Applied Spectroscopy*, Vol.61, pp.479-485, 2007.

80. Garcia de Abajo, F. J., ‘‘Colloquium: Light scattering by particle and hole array’’, *Reviews of Modern Phys*ics, Vol.79, pp.1267-1290, 2007.

81. Abald Cela, S., P. Aldeanueva Potel, C. Mateo, L. Rodriguez Lorenzo, R. A. Alvarez Puebla, L. M. Liz Marzan, ‘‘Surface-Enhanced Raman Scattering biomedical applications of plasmonic colloidal particles’’, *Journal of Royal Society Interface*, Vol.7, pp.435-450, 2010.

82. Willets, K. A., R. P. Van Duyne, ‘‘Localized Surface Plasmon Resonance spectroscopy and sensing’’, *Annual Review of Physical Chem*istry, Vol.58, pp.267-297, 2007.

83. Haes, A. J., R. P. Van Duyne, ‘‘An unified view of propagating and localized surface plasmon resonance biosensors’’, *Analytical and. Bioanalytical Chemistry*, Vol.379, pp.920-930, 2004.

84. Ungureanua, A., D. Trong Ona, E. Dumitriub, S. Kaliaguinea, “Hydroxylation of 1-naphthol by hydrogen peroxide over UL-TS-1 and TS-1 coated MCF”, *Applied Catalysis A*, Vol.254, pp.203–223, 2003.

85. Deegan, R. D., O. Bakajin, T. F. Dupont, G. Huber, S. R. Nagel, T. A. Witten ”Capillary flow as the cause of ring stains from dried liquid drops” *Nature*, Vol.389, pp.827-829, 1997.

86. Fu, Y., H. Wang, R. Shi, J. X. Cheng, “Characterization of photodamage in coherent anti-Stokes Raman scattering microscopy”, *Optics Express*, Vol.14, pp.3942-3951, 2006.

87. Etchegoin, P. G. , P. D. Lacharmoise, E. C. Le Ru, “Influence of Photostability on Single-Molecule Surface Enhanced Raman Scattering Enhancement Factors”, *Analytical Chemistry*, Vol.81, pp.682-688, 2009.